JGR Solid Earth

RESEARCH ARTICLE
10.1029/2024JB029239

The Sierra Madre Oriental Orocline: Paleomagnetism of the Nazas Province in NE Mexico

Rafael Guerra Roel[1,2], Daniel Pastor Galán[2,3,4], Gabriel Chávez-Cabello[5], César Francisco Ramírez-Peña[5], José Jorge Aranda Gómez[6], Gerardo Patiño Méndez[5], R. Giovanny Nova[7], Alejandro Rodríguez-Parra[8], and Roberto Stanley Molina Garza[6†]

[1]Posgrado de la Facultad de Ciencias de la Tierra, Universidad Autónoma de Nuevo León, Linares, Mexico, [2]Facultad de Ciencias de la Universidad de Granada, Universidad de Granada, Granada, España, [3]Consejo Superior de Investigaciones Científicas (CSIC) Doctor Severo Ochoa 7, Madrid, España, [4]Frontier Research Institute for Interdisciplinary Science, Tohoku University, Sendai, Japan, [5]Universidad Autónoma de Nuevo León, Facultad de Ciencias de la Tierra, Linares, Mexico, [6]Universidad Nacional Autónoma de Mexico, Centro de Geociencias, Juriquilla, Mexico, [7]Instituto de Geociências, Universida de São Paulo, São Paulo, Brasil, [8]Ministerio de Minas y Energía, Colombia, Bogotá, Colombia

†Deceased

Key Points:

- With Paleomagnetism we explore the nature of the striking curvature of the Northeastern section of the Mexican Fold-and-Thrust Belt
- Our study shows evidence of Orocline bending or Buckling during the major horizontal crustal shortening event of the Mesozoic in Mexico

Supporting Information:

Supporting Information may be found in the online version of this article.

Correspondence to:

D. Pastor Galán and G. Chávez-Cabello, dpastorgalan@csic.es; gabriel.chavezcbl@uanl.edu.mx

Citation:

Guerra Roel, R., Pastor Galán, D., Chávez-Cabello, G., Ramírez-Peña, C. F., Aranda Gómez, J. J., Patiño Méndez, G., et al. (2024). The Sierra Madre Oriental Orocline: Paleomagnetism of the Nazas province in NE Mexico. *Journal of Geophysical Research: Solid Earth*, *129*, e2024JB029239. https://doi.org/10.1029/2024JB029239

Received 8 APR 2024
Accepted 19 AUG 2024

Author Contributions:

Conceptualization: Rafael Guerra Roel, Daniel Pastor Galán, Roberto Stanley Molina Garza
Data curation: Rafael Guerra Roel, Daniel Pastor Galán, Gerardo Patiño Méndez
Formal analysis: Rafael Guerra Roel, Gerardo Patiño Méndez, R. Giovanny Nova, Alejandro Rodríguez-Parra, Roberto Stanley Molina Garza
Funding acquisition: Rafael Guerra Roel, Daniel Pastor Galán, Gabriel Chávez-Cabello, José Jorge Aranda Gómez, Roberto Stanley Molina Garza
Investigation: Rafael Guerra Roel, Gerardo Patiño Méndez

Abstract

Curved mountain belts are spectacular natural features that contain crucial 3D information about the tectonic evolution of orogenic systems in the absence of other kinematic markers. The Mesozoic units exposed in the Mexican Fold and Thrust Belt in northeastern Mexico show a striking curvature, whose kinematic history has not been studied. The existing tectonic models of the region simply assumed the shape of the tectonic units as an inherent feature to the orogen. We investigated the kinematic history of this curvature through paleomagnetism and rock magnetism analyses, coupled with an exhaustive review of available published literature. The studied data sets indicate a protracted history of (re)magnetizations that occurred during the Late Jurassic-Paleocene times at least during the Late Jurassic, Cretaceous and early Eocene. More significantly, they show significant counterclockwise rotations in the northern flank of the curvature and moderate clockwise vertical axis rotations along its southern flank. This data set suggests that the Sierra Madre Oriental was a linear belt that experienced oroclinal bending or buckling during the Cretaceous to early Eocene period (120–50 Ma).

Plain Language Summary

The geological history of the American Cordillera is complex due to its extensive geological history. We have investigated a section of this Pacific-Panthalassa region: the remarkable curved sector of the Mexican Fold and Thrust Belt in northeastern Mexico. This winding area, known as the Sierra Madre Oriental, potentially holds important clues about the evolution of the North American crust. To contribute to a better understanding of this area and to complement the scarce geophysical and geological studies, we used the magnetic properties of rocks and reviewed existing published research to investigate. We've uncovered a complex history of rock magnetizations with at least two main events dating back to the Late Jurassic and Cretaceous periods. Our findings also reveal that these mountain ranges were rotated from their original position on vertical axes, suggesting they were originally linear and were bent or buckled during the period from approximately 120 to 50 million years ago.

1. Introduction

Orogens, created by the opening and closing of ocean basins, are the most visible product of plate tectonics where continents form and stabilize. Whereas cross-section views are the most valuable source of information to understand orogenesis in 2D, their lateral variations are the best opportunity to understand their kinematic evolution in 3D (e.g., Gutiérrez-Alonso et al., 2008; Pastor-Galán, 2022). Most orogens on Earth are curved to some degree (Johnston et al., 2013; Liu et al., 2023; Marshak, 1988; Weil & Sussman, 2004) and the kinematics of such curvatures have the ability to explain the complex interactions between the evolving stress fields in a mountain belt and its various rock units (e.g., Johnston et al., 2013; Liu et al., 2023; Pastor-Galán, 2022). Understanding the kinematics of those curved mountain belts is crucial to understand large-scale tectonic problems.

The kinematic classifications of orogenic curvatures (Johnston et al., 2013; Pastor-Galán et al., 2017; Sussman & Weil, 2004) distinguish (a) Primary curvatures, which pre-dates the orogenic building (e.g., Jura mountains: Hindle & Burkhard, 1999); and (b) Oroclines (Carey, 1955) that are the product of vertical axis rotations. Oroclines can be classed as progressive oroclines: that is portions of orogens that bend during the main

Methodology: Rafael Guerra Roel, Daniel Pastor Galán, Roberto Stanley Molina Garza
Project administration: Rafael Guerra Roel, José Jorge Aranda Gómez, Roberto Stanley Molina Garza
Resources: Rafael Guerra Roel, Roberto Stanley Molina Garza
Software: Rafael Guerra Roel, Daniel Pastor Galán
Supervision: Rafael Guerra Roel, Daniel Pastor Galán, Gabriel Chávez-Cabello, José Jorge Aranda Gómez, Roberto Stanley Molina Garza
Validation: Rafael Guerra Roel
Visualization: Rafael Guerra Roel, Daniel Pastor Galán, Gabriel Chávez-Cabello, César Francisco Ramírez-Peña, José Jorge Aranda Gómez
Writing – original draft: Rafael Guerra Roel
Writing – review & editing: Rafael Guerra Roel, Daniel Pastor Galán, Gabriel Chávez-Cabello

deformation pulse (e.g., the Talesh; Rezaeian et al., 2020); and secondary oroclines, where the orogen bens or buckles after the main deformation phase (e.g., the New England Oroclines, Li et al., 2012). The mechanisms that form oroclines may involve from the uppermost crust (Marshak, 1988, 2004a, 2004b), to the whole lithosphere (Bagheri & Damani Gol, 2020; Gutiérrez-Alonso et al., 2004; Pastor-Galán et al., 2012). Many structural techniques can inform about the kinematics of curved orogens (Bagheri & Damani Gol, 2020; Hindle & Burkhard, 1999; Kollmeier et al., 2000; Li et al., 2012, 2021; Pastor-Galán et al., 2011, 2014, 2017; Shaanan et al., 2014; Shaw et al., 2012; Weil & Yonkee, 2009; Yonkee & Weil, 2010). However, paleomagnetism is the best tool to do it, as the geomagnetic field is independent of the orogenic deformation (Abrajevitch et al., 2005; Eldredge et al., 1985; Pastor-Galán et al., 2015, 2018, 2020; Weil et al., 2001, 2010, 2013).

The American Cordillera runs along the Pacific coast of the Americas (Figure 1). It encompasses notable mountain belts like the Rockies, Sierra Madre Oriental, and the Andes, as well as extensive plateaus (Colorado, Atacama). The Cordillera includes Pangea derived terranes that have interacted with magmatic arcs, and oceanic plateaus (Guerrero, Baja-BC, Kula Plateau; Keppie, 2004). It also exhibits several striking changes in its trend, such as in Alaska (Johnston, 2001), Panama (Montes et al., 2012), the Colombian Eastern Cordillera (Jiménez et al., 2014), Bolivia (Eichelberger & McQuarrie, 2015), and Patagonia (Maffione et al., 2010). Unraveling the kinematics of these bends is crucial for understanding the Cordilleran geodynamics (e.g., Johnston, 2001). The curvature of the Sierra Madre Oriental in North Central Mexico has often been overlooked. So far only two hypotheses, focused on distributions of Early Jurassic igneous rocks and red beds, tried to explain the curved pattern: (a) As product of large-scale left-lateral faulting during the Late Jurassic (Anderson & Schmidt, 1983; Anderson et al., 2005; Jones et al., 1995; Molina-Garza & Iriondo, 2005; Silver & Anderson, 1974), and (b) a general assumption of a primary curvature resulting from the a curved segment of the subduction zone (Barboza-Gudiño et al., 2008, 2014; Dickinson & Lawton, 2001; Godínez-Urban et al., 2011; Lawton & Molina Garza, 2014; Martini & Ortega-Gutiérrez, 2018; Molina-Garza et al., 2020; Stern & Dickinson, 2010).

Although relatively well known in cross section (e.g., Fitz-Díaz et al., 2018 and references therein), the Sierra Madre Oriental critically lacks data informing about the kinematics of its curvature. Pioneering paleomagnetic studies in the area described vertical axis rotations (Belcher, 1979; Clement et al., 2000; González-Naranjo et al., 2012; Göse et al., 1982; Kleist et al., 1984; Molina Garza, 2004; Nemkin et al., 2019; Nowicki et al., 1993; Warrior, 2008), however, they were not focused on understanding rotations but on obtaining information on paleolatitudes or magnetostratigraphy. In this paper, we investigate the nature of the curvature of the Sierra Madre Oriental through new paleomagnetic data from Jurassic units (Nazas, La Joya and La Boca formations) and critically review previous studies along the curved section of the Sierra Madre Oriental.

2. Geological Setting

The Mesozoic tectonic history of Mexico is coupled with break-up of Pangea and the eastward subduction of Paleo-Pacific plates under North America (Boschman et al., 2018; Fitz-Díaz et al., 2018 and references therein). From Late Triassic to earliest Cretaceous, the effects of the breakup of Pangea perhaps combined with extension related to the roll-back of the Paleo-Pacific in western Pangea formed a series of continental, and marine basins (Barboza-Gudiño et al., 2021; Busby et al., 2023; Martini & Ortega-Gutiérrez, 2018; Pindell & Kennan, 2001). One of those basins is the Nazas province (e.g., Barboza-Gudiño et al., 2008; Busby & Centeno-García, 2022; Martini & Ortega-Gutiérrez, 2018). The Nazas province includes sedimentary rocks, with subordinate volcano-sedimentary rocks and lava flows deposited from the beginning of the Jurassic (~200 Ma) to the Callovian (~165 Ma) (Barboza-Gudiño et al., 2008; Bartolini et al., 2003; Busby & Centeno-García, 2022). The continued extensional setting during the Oxfordian (~160 Ma) triggered a large marine transgression responsible for the accumulation of a ~5 km thick marine sedimentary succession (hereafter "sedimentary cover"; Bartolini et al., 1999; Goldhammer, 1999; Gray & Lawton, 2011; Hernández-Romano et al., 1997; Ocampo-Díaz et al., 2016). After The Guerrero Terrane accretion (~120 Ma) the sedimentary rocks of the Mesozoic Basin of Central Mexico deformed forming the Mexican Fold and Thrust Belt, typically defined as the foreland of the Mexican orogen (e.g., Busby et al., 2023; Fitz-Díaz et al., 2018).

The Mexican Fold and Thrust Belt developed over a regional decollement (i.e., "thin-skinned" tectonics) where the sedimentary cover was transported northeast (Eguiluz et al., 2000; Fitz-Díaz et al., 2018 and references therein). The age of regional folding in the hinterland of the Mexican Fold and Thrust Belt (Fitz-Díaz et al., 2016; Gutiérrez-Navarro et al., 2021; Williams et al., 2021), syntectonic magmatism (Teyra and Peñuelo plutons

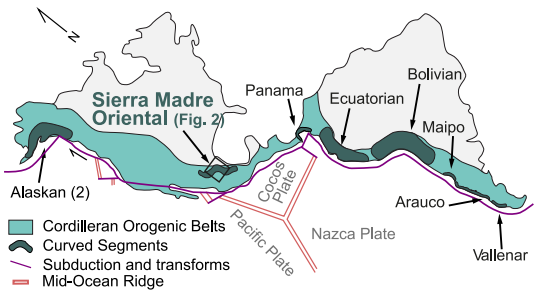

Figure 1. The American Cordilleran Orogenic Belt and some of the curved segments along its trace. The black square is the location of the study area (Modified from DeCelles et al. (2009)).

Ramírez-Peña & Chávez-Cabello, 2017) and synorogenic clastic sedimentation (Concepción del Oro Formation; Fitz-Díaz et al., 2018; Ocampo-Díaz et al., 2016) has been bracketed between 90 and 50 Ma. The Mexican Fold and Thrust Belt contains several recesses and salients that may reflect the original geometry of the coastline and the geographic distribution of the basement highs (Monterrey, Figure 2; e.g., Chávez-Cabello et al., 2004; Nemkin et al., 2019; Padilla y Sánchez, 1985; Zachary, 2012). In localized areas along the trace of the Mexican Fold and Thrust Belt late high-angle reverse faults cut the older folds and thrusts and expose Jurassic volcano-sedimentary strata and, in some cases, Paleozoic basement (Chávez-Cabello et al., 2005; Fitz-Díaz et al., 2018; Guerra Roel, 2019; Gutiérrez-Navarro et al., 2021; Mauel et al., 2011; Ramírez-Peña & Chávez-Cabello, 2017; Ramírez-Peña et al., 2019; Zavala-Monsiváis et al., 2012; Zhou et al., 2006). To our knowledge, no kinematic analyses have been performed in the Sierra Madre Oriental to understand the curvature's kinematics. However, there have been speculations about the curved distribution of the outcrops in the Nazas province. Some authors have interpreted this curvature as the result of large-scale transcurrent faults that fragmented and displaced Mexico (Anderson & Schmidt, 1983; Anderson et al., 2005; Jones et al., 1995; Molina-Garza & Iriondo, 2005; Silver & Anderson, 1974). Others have suggested that Nazas' curved distribution represents its original formation parallel to a hypothetical curved subduction zone (Barboza-Gudiño et al., 2008, 2014, 2021; Dickinson & Lawton, 2001;

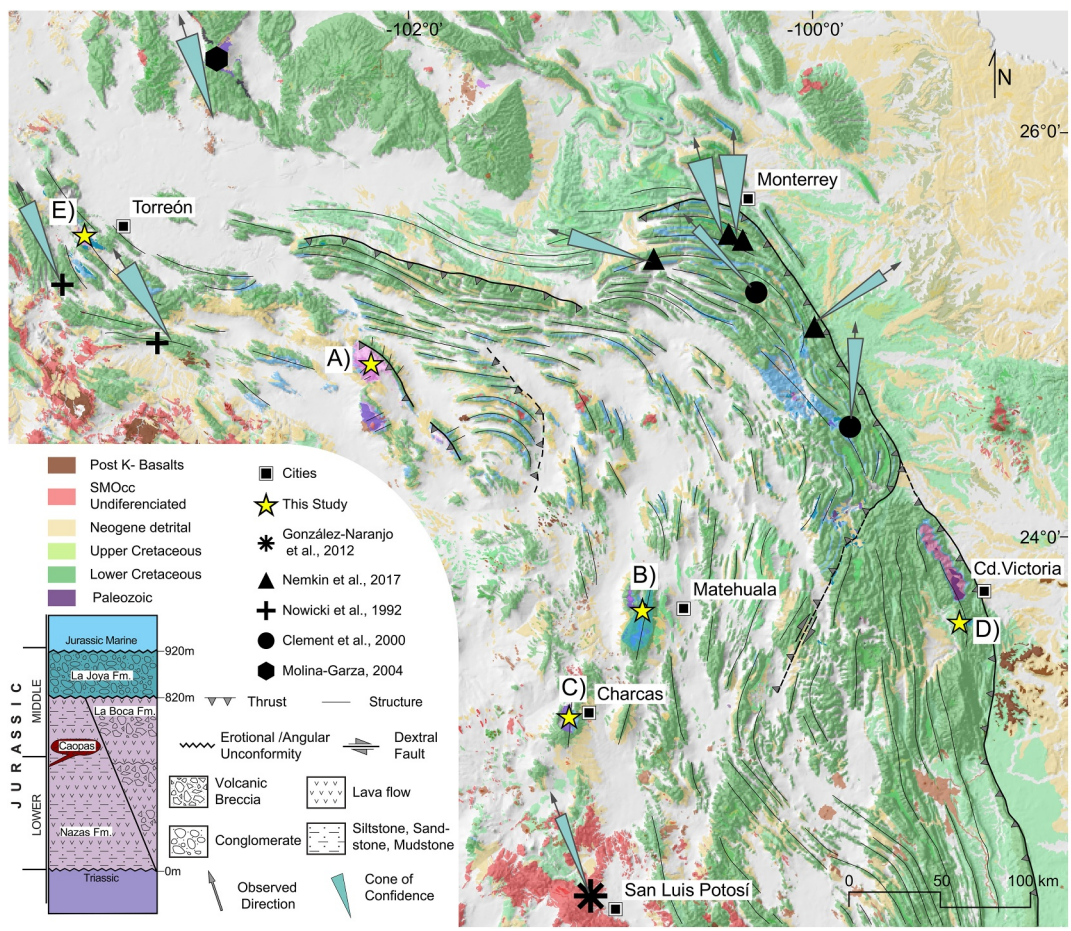

Figure 2. Synthetic geological map and general structural trend of main structures in the Sierra Madre Oriental. Regional distribution of the localities sampled areas is as follows. (A) San Julián Uplift, (B) Real de Catorce, (C) Charcas, (D) Huizachal Valley, (E) Villa Juárez. Black symbols represent the accepted localities/directions from the literature (Modified from open-source vector data from INEGI (2023) and SGM (2023)).

Godínez-Urban et al., 2011; Lawton & Molina Garza, 2014; Martini & Ortega-Gutiérrez, 2018; Stern & Dickinson, 2010).

2.1. The Nazas Formation

The Nazas Formation (Fm.) is a succession of thick siliciclastic sediments interbedded with subordinate lava flows, ignimbrites, and volcanic breccias of andesitic to rhyolitic compositions (Barboza-Gudiño et al., 2021; Busby & Centeno-García, 2022; Lawton & Molina Garza, 2014; Pantoja-Alor, 1972 and references therein). Its thickness is variable and ranges from 250 to 820 m (Clemons & McLeroy, 1965; Eguiluz-de Antuñano et al., 2014; Lawton & Molina Garza, 2014; Pantoja-Alor, 1972). The type locality of the Nazas Fm. is in Cerritos Colorados near Villa Juárez, Durango (Figure 2E; Lawton & Molina Garza, 2014; Pantoja-Alor, 1972). Some hypabyssal bodies with intermediate chemical composition and similar age have been attributed to the Nazas Fm. (Barboza-Gudiño et al., 2021; Jones et al., 1995; López-Infanzón, 1986). These intrusive bodies have been interpreted both as a rift setting related to the break-up of Pangea (Busby & Centeno-García, 2022; Martini & Ortega-Gutiérrez, 2018) and arc-derived rocks (Barboza-Gudiño et al., 2008, 2021; Bartolini et al., 2003; González-León et al., 2021; Mauel et al., 2011; Zavala-Monziváis et al., 2012). Busby and Centeno Garcia (2022) summarized all the reported ages of the Nazas formation and all the possible known correlatable igneous rocks in the US and NW Mexico. The oldest reported ages for the Nazas formation are 193.3 ± 1.5 (U-Pb LA-ICP-MS in zircon; Barboza-Gudiño et al., 2021; Busby & Centeno-García, 2022 and references therein) to as young as 158 ± 4 (Busby & Centeno-García, 2022; Jones et al., 1995 and references therein).

2.2. Jurassic Red Beds

The Nazas Fm. changes laterally and is overlain with a Jurassic pre-Oxfordian sedimentary succession of red sandstone, siltstone, conglomerate, breccia, and volcaniclastic reddish beds (Busby & Centeno-García, 2022; Zavala-Monsiváis et al., 2012). These materials were deposited in continental to marine transitional environments. Two formations have been defined: La Joya and La Boca Formations which are commonly addressed as Jurassic red beds (Barboza-Gudiño et al., 2008, 2010; Fastovsky et al., 2005; Imlay et al., 1948; Mixon et al., 1959; Rubio-Cisneros et al., 2011). The La Boca Formation is a lateral to overlying variation of the Nazas Fm. (Rubio-Cisneros & Lawton, 2011; Zavala-Monsiváis et al., 2012). It has two informal members that are separated by an angular unconformity that ranges from a few degrees (10–20°) to 70° locally in the Huizachal Valley, an angle that increases in the vicinity of rhyolite intrusions (Rubio-Cisneros & Lawton, 2011). The (a) lower member consists of lapilli tuffs, lava flows, volcanic breccias, and ignimbrites interbedded in greater proportion with volcaniclastics and detritus derived primarily from coeval volcanic rocks that represent deposits from the Nazas volcanic activity (Rubio-Cisneros & Lawton, 2011). The volcanic component in the La Boca Formation gradually decreases toward the top of the stratigraphic unit. The (b) upper informal member of this formation is mostly red siliciclastic strata. These rocks fine upwards in a conglomerate, sandstone, and siltstone succession (Fastovsky et al., 2005). The reported maximum depositional age (youngest detrital zircon) for the La Boca Formation is 184–183 Ma for the lower member and 167 Ma for the upper member (Rubio-Cisneros & Lawton, 2011). La Boca Formation and the Nazas Fm. are overlain by La Joya Formation, a siliciclastic unit with a basal fining upward conglomerate to reddish siltstone and mudstone. It was deposited in continental to a marginal marine environment with subordinate freshwater limestone and is overlain by the upper Jurassic-Paleogene marine sedimentary cover that starts with the Oxfordian Minas Viejas evaporites (Padilla y Sánchez, 1985; Rubio-Cisneros & Lawton, 2011; Salvador, 1987). The youngest detrital zircon ages of La Joya Formation are 166.2 ± 1.9 Ma at the top of this unit in Real de Catorce (Barboza-Gudiño et al., 2012), and 158.36 ± 1.2 in the La Ballena area (Wengler et al., 2019) in Huizachal Valley was bracketed as Callovian in age (Rubio-Cisneros & Lawton, 2011). During the last recorded episode of horizontal crustal shortening of the Mexican Fold and Thrust Belt (Upper Cretaceous-Eocene), the Jurassic red beds and the Nazas Fm. were exhumed by high-angle reverse faults that disrupted the predeceasing structures (Thick-skinned tectonics; e.g., San Julian Uplift "A" in Figure 2; Fitz-Díaz et al., 2018; Ramírez-Peña & Chávez-Cabello, 2017; Ramírez-Peña et al., 2019; Williams et al., 2021) and in some areas developed antiformal stack structures (Figure 2B; Gutiérrez-Navarro et al., 2021).

3. Paleomagnetism in the Sierra Madre Oriental

Paleomagnetic studies in the curved sector of the Sierra Madre Oriental are scarce. We thoroughly reviewed the published literature and identified only nine research documents containing paleomagnetic directions in Mesozoic

to Oligocene rocks (Belcher, 1979; Clement et al., 2000; González-Naranjo et al., 2012; Göse et al., 1982; Kleist et al., 1984; Molina Garza, 2004; Nemkin et al., 2019; Nowicki et al., 1993; Warrior, 2008) (see Table 1 and Table S1 in Supporting Information S1). From these studies, six of them suggested vertical axis rotations of variable magnitudes (Clement et al., 2000; Göse et al., 1982; Kleist et al., 1984; Nemkin et al., 2019; Warrior, 2008). However, all of the rotations were considered as local features (e.g., Nemkin et al., 2019; Warrior, 2008) or even spurious (e.g., Clement et al., 2000). Unfortunately, none of the data sets disclose data to the specimen level and therefore they cannot be faithfully re-interpreted. The reviewed studies do provide site or locality averages. To evaluate the reliability and trustworthiness of the presented data sets, we have established a series of quality criteria for the data following the most recent paleomagnetic consensus (Gerritsen et al., 2022; Meert et al., 2020; Sapienza et al., 2023). We discarded sites/localities when one of the following criteria was not satisfied: (a) Specimens were stepwise demagnetized; (b) directions were obtained by principal component analysis of at least 4 points; (c) Sufficient structural data and field tests were provided (fold, conglomerate, or baked contact test) to allow us to establish a relative timing of magnetization; (d) Sites with more than three specimens show $k > 40$ (otherwise they may not represent a single spot reading of the geomagnetic field); (e) localities consist of at least 7 independent spot readings of the geomagnetic field; (f) Localities show $10 < k < 85$ (poor concentration parameter k may indicate structural or magnetization problems and very high k are likely to represent spot readings). In some cases, we performed a parametric resampling (Deenen et al., 2011; Koymans et al., 2016) to re-evaluate the effectiveness of the field tests provided by the authors (i.e., Nemkin et al., 2019) or to average out repetitive localities that were too close to each other and showed consistent values (i.e., Molina Garza, 2004). Nowicki et al. (1993) reported four localities that do not pass a fold-test from Lower Cretaceous units near the area of Torreon Coahuila in the Sierra Madre Oriental (Figure 2). After applying the criteria only two localities (Localities 2 and 4) were accepted from this work (see Table 1 and 1). Clement et al. (2000) mention several localities but unfortunately only report two of them in the Sierra Madre Oriental. They both account for a positive fold test and reversals and are considered primary (ca. 130 Ma). Although the structural data provided would not be enough to pass our criteria, we could retrieve structural data from the sampled outcrops from Chávez-Cabello et al. (2011). Both localities of Clement et al. (2000), give almost opposite declinations without changes in inclination. After reviewing Chávez-Cabello et al. (2011) we conclude that such a significant vertical axis rotation is local and due to a strike-slip fault. Nemkin et al. (2019) report several localities along the trace of the Monterrey salient of the Sierra Madre Oriental. The results were interpreted as post and syn-folding in origin. However, in some of the cases fold axes plunge steeply, which hinders both the interpretation of the fold test and the declinations. From their extensive data set, only four localities passed the criteria. To avoid relying on previous interpretations, and since structural data was properly addressed, we performed the fold tests (Tauxe & Watson, 1994) again using the provided data and also parametrically resampling it (Tauxe, 2010; Tauxe & Watson, 1994). We found that the fold test containing localities 4–6 from Nemkin et al. (2019) was better interpreted as post-folding rather than 35% syn-folding. The differences in declination between both analyses are, however, not significant (Table 1 and Table S1 in Supporting Information S1).

The different Triassic sites studied by Molina Garza (2004) that passed the criteria were averaged out as a single locality. These directions count with a baked contact test and show very similar directions with Paleozoic overlying strata. González-Naranjo et al. (2012) collected 368 oriented core samples in 50 sites in the Panalillo Ignimbrite (Oligocene in age). 20 of the sites passed the quality criteria and were averaged out as a single locality. All localities that passed the criteria were processed and are listed in Table 1 and shown in Figure 2. The remaining sites were excluded from any further analyses (see Table S1 in Supporting Information S1 for details).

4. Sampling and Methods

4.1. Sampling Strategy

Our collected samples came from outcrops of the Nazas, La Joya and La Boca formations in central and NE Mexico (e.g., Barboza-Gudiño et al., 2004; Busby & Centeno-García, 2022). We collected a total of 620 core samples of 2.5 cm diameter with a gas-powered drill and oriented them with a Pomeroy orienting fixture and a Brunton Pocket Transit compass. 355 cores come from the Nazas Fm. and the remainder 265 from the red bed formations. In some localities, we also collected oriented blocks and later drilled them in the laboratory. The samples were collected in localities representing different trends of the Sierra Madre Oriental curvature (stars in Figure 2, letters of locality correspond with the descriptions below).

Table 1
Final Mean Directions Used for Interpretation in Geographic and Tectonic Coordinate Systems

										A95					Coordinates			
		N	Ns	mDec	mInc	k	a95	K	A95	Min	Max	ΔDx	ΔIx	Pole lng	Pole lat	Lat.	Long.	R	ΔR
Geographic																			
(A)	Mina San Miguel	91	101	285.76	20.95	10.15	4.9	17.5	3.65	1.97	4.78	3.72	6.6	175.72	16.44	24.89	−102.15	−60.65	5.49
	Caopas*	51	69	270.73	17.59	10.1	6.61	13.4	5.66	2.49	6.89	5.73	10.54	180.79	5.38	24.83	−102.20	−75.34	6.68
	Nazas North*	24	32	261.63	26.74	8.37	10.89	7.94	11.21	3.37	11.07	11.57	19.02	190.08	−2.68	24.94	−102.24	−73.94	9.54
(B)	Real de Catorce	89	91	346.91	42.95	41.41	2.36	37.13	2.49	1.99	4.85	2.75	3.25	185.05	77.02	23.70	−100.89	3.11	3.45
(C)	Charcas	41	41	22.02	−5.05	52.98	3.1	75.96	2.58	2.72	7.9	2.58	5.13	36.02	56.55	23.10	−101.17		
(D)	Huizachal	75	89	337.07	20.87	13.8	4.57	22.65	3.52	2.13	5.4	3.58	6.36	151.59	57.74	23.59	−99.23		
	NEM4-6	21	21	3.39	31.1	29.17	5.99	37.23	5.28	3.55	12.05	5.51	8.45	60.92	82.04	24.91	−99.93		
	NEM-12/13	15	15	356.91	49.29	25.87	7.66	20.89	8.57	4.06	14.89	9.92	9.75	233.61	83.45	25.49	−100.36		
	NEM-24/25	10	10	343.61	54.16	79.55	5.45	49.51	6.93	4.78	19.22	8.44	7.03	207.46	72.93	25.48	−100.42	2.50	8.79
	NEM-26/27	13	13	287.84	44.68	69.29	5.02	73	4.88	4.3	16.29	5.45	6.15	188.07	26.21	25.39	−100.80	−53.09	6.97
	CLE-SR	86	91	55.31	37.58	13.87	4.25	14.47	4.16	2.02	4.96	4.45	5.99	339.11	41.19	25.10	−100.22	72.09	4.47
	CLE-CT	47	47	317.06	45.44	50.96	2.94	43.72	3.18	2.57	7.25	3.57	3.94	182.96	51.66	25.10	−100.33	−25.70	4.29
	NOW-LOC2	27	27	336.79	44.16	31.24	5.05	26.91	5.46	3.21	10.28	6.07	6.94	175.02	69.03	25.27	−103.77		
	NOW-LOC4	10	10	328.16	37.89	41.47	7.59	47.4	7.09	4.78	19.22	7.61	10.17	167.17	61.09	24.98	−103.25		
	MG	8	9	341.63	3.94	30.79	10.14	49.41	7.96	5.22	22.12	7.96	15.86	110.53	60.65	26.50	−103.00	−7.35	10.64
	GN	22	22	339.73	31.62	52.83	4.3	69.16	3.75	3.49	11.7	3.93	5.96	159.26	70.36	22.10	−101.00		
Tectonic																			
(A)	Mina San Miguel	73	101	294.81	35.17	7.45	6.53	8.79	5.94	2.16	5.49	6.3	8.92	185.79	32.91	24.89	−102.15		
	Caopas*	51	69	270.73	17.59	10.1	6.61	13.4	5.66	2.49	6.89	5.73	10.54	180.79	5.38	24.83	−102.20		
	Nazas North*	25	37	262.96	27.46	12.89	8.39	14.45	7.89	3.31	10.79	8.15	13.26	195.26	−9.64	24.94	−102.24		
(B)	Real de Catorce	85	91	326.73	39.72	9.81	5.17	13.52	4.34	2.03	4.99	4.7	6.02	182.15	56.07	23.70	−100.89		
(C)	Charcas	41	41	20.35	30.7	52.74	3.1	75.87	2.58	2.72	7.9	2.69	4.15	3.04	69.79	23.10	−101.17	25.44	3.90
(D)	Huizachal	78	89	333.16	27.02	10.17	5.29	15.86	4.16	2.1	5.27	4.29	7.03	162.1	57.42	23.59	−99.23	−10.74	6.48
	NEM4-6	14	21	9.83	−22.27	30.39	7.33	66.48	4.91	4.18	15.55	5.01	8.76	110.55	59.37	24.91	−99.93	14.56	7.03
	NEM-12/13	15	15	356.91	49.29	25.87	7.66	20.89	8.57	4.06	14.89	9.92	9.75	233.61	83.45	25.49	−100.36	8.48	10.57
	NEM-24/25	10	10	343.61	54.16	79.55	5.45	49.51	6.93	4.78	19.22	8.44	7.03	207.46	72.93	25.48	−100.42		
	NEM-26/27	13	13	287.84	44.68	69.29	5.02	73	4.88	4.3	16.29	5.45	6.15	188.07	26.21	25.39	−100.80		
	CLE-SR	86	91	55.31	37.58	13.87	4.25	14.47	4.16	2.02	4.96	4.45	5.99	339.11	41.19	25.10	−100.22		
	CLE-CT	47	47	317.06	45.44	50.96	2.94	43.72	3.18	2.57	7.25	3.57	3.94	182.96	51.66	25.10	−100.33		
	NOW-LOC2	27	27	336.79	44.16	31.24	5.05	26.91	5.46	3.21	10.28	6.07	6.94	175.02	69.03	25.27	−103.77	−6.86	7.62
	NOW-LOC4	10	10	328.16	37.89	41.47	7.59	47.4	7.09	4.78	19.22	7.61	10.17	167.17	61.09	24.98	−103.25	−16.84	10.86
	MG	8	9	341.63	3.94	30.79	10.14	49.41	7.96	5.22	22.12	7.96	15.86	110.53	60.65	26.50	−103.00		
	GN	22	22	339.73	31.62	52.83	4.3	69.16	3.75	3.49	11.7	3.93	5.96	159.26	70.36	22.10	−101.00	−10.79	6.88

Note. All localities are shown as normal polarity. N number of demagnetized specimens, Ns number of specimens that passed the Cutoff, mDec mean declination, mInc mean inclinationg, k precision parameter, a95 radius of the 95% confidence cone about site-mean direction, K precision paramenter of the poles, A95 radius of 95% confidence circle around paleomagnetic pole, A95 min and A95max describe the minimum and maximun values of A95 allowed to considered the average representative. ΔDx, uncertainty in declination; ΔIx, uncertainty in inclination, R observed rotation in reference to the asumed time of magnetization adquisition. + (−Counter) Clockwise. A, B, C, D are referenced in Figures 2, 8, and 9 * Locality shows high VGP elongation see text for detail. (NEM: Nemkin et al., 2019; CLE: Clement et al., 2000; NOW = Nowicki et al., 1993; MG = Molina Garza, 2004; GN = González-Naranjo et al., 2012).

(A) *San Julián Uplift (24.837°N, −102.174°E)*

The San Julian Uplift is a structural block that exposes the stratigraphic boundary between the sedimentary cover and the Nazas Fm. and the largest outcrop of the Nazas Fm. in Mexico. The block was exhumed during the Eocene-Oligocene thick-skinned tectonic event (Guerra Roel, 2019; Ramírez-Peña, 2017; Ramírez-Peña & Chávez-Cabello, 2017). The "thick-skinned" faults cut in high angles the pre-existing curved structure of the Cretaceous "thin-skinned" folds and thrusts (Figure 2). In this area, the Nazas province is represented by the Nazas Fm. (Figures $S1A_1$ and $S1A_3$ in Supporting Information S1), and the Caopas laccolith body (Figure $S1A_2$ in Supporting Information S1) (Nazas Fm. In this area the Nazas Fm. shows foliation and low metamorphic grade of greenschist facies with chlorite). The zircon U-Pb age for the Nazas Fm. in this locality is 174 ± 2 Ma (Ramírez-Peña, 2017). The Caopas laccolith corresponds to a Middle Jurassic hypabyssal body of intermediate composition emplaced in the Nazas Fm.. This body shows a porphyritic texture and, in its upper part, evidence of dynamic metamorphism (porphyroblasts and mineral lineation; Figure $S1A_2$ in Supporting Information S1). The Caopas intrusive yielded a U-Pb zircon age of 165 ± 3 Ma (Ramírez-Peña, 2017). From this area, we collected 256 samples in three separate localities: Mina San Miguel (coded MSM), Nazas North (ALI, NRN), and the Caopas intrusive body (MIC, MIR, MIRN; Table S2 in Supporting Information S1) and the Nazas N locality was sampled in the northern part of the uplift. All the samples belonging to the MSM area and sites Mic1, Mic2, and Mic3 of the Caopas intrusive were drilled in situ (10–15 samples per site). The rest of the sites of the Caopas area (Mic4–Mic7) were collected as oriented blocks (one per site). From each block, we obtained four cores in the laboratory. The poor outcrop exposure of the lava flow succession in the MSM and Nazas N areas, together with their thickness (20–30 m), weathering conditions, and compositional and textural similarities among flows made the task of identifying individual lava flows a challenge. The samples corresponding to the Mina San Miguel were collected in an anticline trend/plunge of 142°/10° that is oblique to the main East-West trend of the structures in the transversal sector of the Mexican Fold and Thrust Belt, at the eastern border of the San Julián Uplift (Figure 2A).

(B) *Real de Catorce (23.621°N, −100.855°E)*

In this locality, the older rocks crop out in the core of an antiformal stack that formed between 91 and 53 Ma ($^{40}Ar/^{39}Ar$ age in illite; Gutiérrez-Navarro et al., 2021). Locally the Nazas Fm. unconformably rests atop Triassic clastic rocks of the Potosí fan (Centeno-García et al., 2005; Silva-Romo et al., 2000) and yielded U-Pb zircon age of 174.7 ± 1.3 Ma (Barboza-Gudiño et al., 2012). The La Joya Fm. lies unconformably over the Nazas Fm. and shows deformation features that suggest that it acted as a decollement, which was developed in the Late Cretaceous during the thin-skinned deformation event (Gutiérrez-Navarro et al., 2021). We sampled 103 cores each in a single fine-grained bed from a 60 m thick succession of sandstones. The samples were distributed in 16 groups labeled RC11–RC26 (Figures S2B and S2D in Supporting Information S1).

(C) *Charcas, San Luis Potosí (23.131°N, −101.188°E)*

The Nazas Fm. in Charcas was dated (U-Pb in zircon) in 179 ± 1 Ma (Zavala-Monsiváis et al., 2012). The structure and tectonic mechanisms have not been studied in detail in this locality, simply described as an anticlinorium, but the structure is in the same crustal block as the Real de Catorce locality.

In this locality we collected samples along the San Antonio River covering about 80 m of the exposed stratigraphic succession of the Nazas Fm. (Figure S2C in Supporting Information S1). We collected 60 cores from 10 sites of the Nazas Fm. labeled CHA-1 to CHA-10 that cover four different andesitic lava flows, interbedded tuff, and epiclastic deposits. Each sampled site corresponds to distinct units no thicker than 2 m, except for sites CHA-1 and CHA-2 which were collected from a single epiclastic deposit.

(D) *Huizachal Valley (23.588°N–99.222°E)*

The locality contains outcrops of the Nazas Fm. in the core of a structural dome and is overlain by the Jurassic red beds of the La Boca and La Joya Formations (Rubio-Cisneros & Lawton, 2011). .Detrital zircon analysis in this locality places the maximum deposition age of the La Boca Formation at ∼190 Ma (Rubio-Cisneros & Lawton, 2011). We drilled 105 samples from La Joya and La Boca Formations in this locality. The sampled formations crop out at the core of an anticline along the valley. Seven sites, with a total of 45 samples, labeled HUI42–HUI48 correspond to La Boca Formation, which consists of fine to coarse red sandstones. Samples were collected in the middle portion of the upper member, closer to the anticline axis. 62 cores distributed in nine sites labeled HUI28–HUI40 were collected from the La Joya Formation on the northwestern limb of the anticline, in an outcrop that

lays along a secondary dirt road approximately 1 km SW from the previously sampled La Boca Formation. Each site sampled comprises a single stratum of about 2 m thick.

(E) *Villa Juárez, Durango (25.501°N, −103.621°E)*

The local age of the volcanic rocks of the Nazas Fm. in this locality is 182.9 ± 2.5 Ma (Barboza-Gudiño et al., 2021). We collected 2–3 oriented blocks in each of the 17 sites (labeled NA01-NA17) from 4 individual andesitic lava flows. We obtained a total of 85 cores from the oriented blocks. Lava flows are interbedded with volcano-sedimentary rocks. The sampled blocks were collected in the limbs of the Villa Juárez anticline (axis' trend/plunge = 315°/18°) which do not show evidence of penetrative deformation (Figures S2E and S2F in Supporting Information S1). Although the precise age of the folding is unknown, the structure is attributed to thin-skinned deformation coupled with the buttressing effect of the Coahuila block, an adjacent basement high. Sediments accumulated in the basin were thrusted over the southern margin of the continental block during the Late Cretaceous (Lawton & Molina Garza, 2014).

4.2. Methods

We selected representative samples for rock magnetism, scanning electron microscope imaging and anisotropy of the magnetic susceptibility. We analyzed all samples to obtain paleomagnetic directions.

4.2.1. Rock Magnetism

Isothermal Remanent Magnetization (IRM) curves and Hysteresis loops were obtained at the Paleomagnetism and Magnetism Laboratory at the Centro de Geociencias of the Universidad Nacional Autonoma de Mexico. The procedure was carried out using an in-house built impulse magnetizer (fields up to 5 T) and in some cases, a Micromag model 2900 with 2 T magnets, Princeton Measurements Corporation, noise level 2×10^{-9} Am^2. The acquired magnetization from the impulse magnetizer was measured in a JR6 spinner magnetometer from AGICO. In this process, we induced an IRM in a progressively increasing field (20–2,900 mT) and afterward, we applied a back-field demagnetization in a progressive order (10–700 mT) following the method described by Kruiver et al. (2001). The Micromag IRM tests were carried out at room temperature and a field of 1 T was applied gradually in 10 mT increments. As for the hysteresis loops the maximum applied field was 1 T in increments of 20 mT on an average time of 600 ms. Sample mass ranged from 40 to 50 mg and were measured using a P1 phenolic probe. IRM curves were unmixed using the MAX Unmix web application (Maxbauer et al., 2016) to determine the main magnetic minerals contributing to the cumulative IRM.

The thermomagnetic curves were obtained in different labs. The Villa Juárez locality was analyzed at the Ivar Giæver Geomagnetic Laboratory (University of Oslo) on a Kappabridge AGICO MFK1-FA equipped with a CS-4 furnace and processed with Cureval8 (AGICO) (Chadima & Hrouda, 2009) and were corrected for stability values and density. We measured the magnetic susceptibility in runs from 0° to 700°C. The San Julián locality, was measured in an in-house built horizontal translation type Curie balance with a sensitivity of approximately 5×10^{-9} Am^2 in the Paleomagnetism and Rock Magnetism Laboratory of the Centro de Geociencias, Universidad Nacional Autonoma de Mexico (UNAM, Queretaro). Due to the small amounts of magnetic material in some of the samples, the tests were carried out on concentrates previously separated using hand magnets. Between 300 and 400 mg of ground, sample was used for each experiment. The Curie balance was programmed to continuously heat the sample to 700°C and gradually cool to room temperature at heating and cooling rates of approximately 10°C min^{-1}.

4.2.2. Anisotropy of the Magnetic Susceptibility and Scanning Electron Microscopy

We used Anisotropy of Magnetic Susceptibility (AMS) as a proxy for describing deformation in weakly deformed rocks (e.g., Parés, 2015; Weil & Yonkee, 2009). The shape of the AMS ellipsoid (graphically represented with its three axes: $k_{max} > k_{int} > k_{min}$) depends on different features such as the orientation of mineral grains, compositional layering, the crystallographic orientation of individual minerals, distribution, and size of microfractures, and the grain shape and size (e.g., Butler, 1992; Tarling & Hrouda, 1993). The analyses were carried out in a Kappabridge model KLY-3 in the Paleomagnetism and Rock Magnetism Laboratory of the Centro de Geociencias, Universidad Nacional Autonoma de Mexico (UNAM) in Juriquilla Queretaro, Mexico. We present the AMS ellipsoid in terms of equal area projection and shape parameter graphs both Flinn (1962) and Jelinek (1981).

We analyzed several samples using a Scanning Electron Microscope (SEM) model TM-1000 Hitachi equipped with energy-dispersive X-ray spectroscopy (EDS: Oxford). This procedure was done in the Laboratory of Crustal Fluids in the Centro de Geociencias, Universidad Nacional Autonoma de Mexico (CEGEO UNAM, Queretaro).

4.2.3. Paleomagnetism

All samples were progressively demagnetized using thermal (TH) or alternating fields (AF) demagnetization procedures. The processing of the samples collected for this work was carried out in different laboratories. The Villa Juárez Locality was measured in the shielded room of the Ivar Giæver Geomagnetic Laboratory in Norway, which is equipped with a furnace model MMTD8oA for TH,an AF degausser LDA-3A and a superconducting rock magnetometer WSGI model 755 (2G Enterprises). Part of the Samples from the Charcas, Real de Catorce and Huizachal Valley were demagnetized in the University of Texas at Dallas (UTD, Geoscience Department Paleomagnetism and Rock Magnetics Lab) using a cryogenic magnetometer 2G Enterprises, using AF as method. The rest of the localities were demagnetized in the Paleomagnetism and Rock magnetism laboratory in the Centro de Geociencias, UNAM, Queretaro, using a shielded furnace with a heating capacity of up to 640°C and a AGICO JR-6 spinner magnetometer. The remanent magnetization was measured using an AGICO JR-6 spinner magnetometer.

The paleomagnetic directions were analyzed with Paleomagnetism.org software (Koymans et al., 2016, 2020), which uses principal component analysis to define magnetic components (Kirschvink, 1980) and Fisher (1953) statistics to calculate averages and errors in directions and virtual geomagnetic poles (VGPs). We have represented the directions graphically in both Zijderveld (1967) and equal area projection diagrams. We have considered as a direction only those with five or more demagnetization steps in line and maximum angular deviation (MAD) <15° (McElhinny & McFadden, 1999). We applied a 45° cut-off in each site to discard outlying points. We also used the McFadden and McElhinny (1988) method of combining great circles and best-fitted set point directions for samples where components were difficult to isolate. Two localities allow for a fold test (MSM and Real de Catorce localities).

Additionally, the reliability of each data set was tested with Deenen et al. (2011) criterion that evaluates the scatter of VGPs. This criterion denotes that when the VGP scatter can be attributed solely to paleosecular variation (PSV), the VGP distribution tends to be circular. Nonetheless, unaccounted structural corrections, inclination shallowing, and or vertical axis rotations may add additional scatter (i.e., ellipticity) to the associated distribution. Finally, to test the reliability of data from unique lava flows, we have compared the differences between the average of site means within a locality against the average of all individual directions.

5. Results

5.1. San Julian Uplift

5.1.1. IRM and Hysteresis

The IRM results show noisy curves and are similar for most of the samples. The minerals that hold the NRM for the volcanic samples reach saturation in the range below 400 mT. suggesting that their remanence is controlled by ferrimagnetic phases (probably Ti-magnetite; Gubbins & Herrero-Bervera, 2007; Figures S3a and S3b in Supporting Information S1). We measured 26 representative samples. The coarse grain texture of the Caopas laccolith along with the scarcity of magnetic minerals resulted in noisy results (dia-/para- magnetic) for the intrusive rock samples. Although the curves did not reach saturation at 1 T, both interpretable results show hysteresis loops that resemble those of superparamagnetic magnetite (grain size <10 nm; Dunlop & Özdemir, 1997) with a possible minor content of a hard phase (likely hematite: Figure 3a). The NRN sites of the sampled andesites from Nazas North area show a hysteresis loop with a high coercivity phase that does not saturate at 1 T (Figure 3b), we interpret this phase as hematite (Gubbins & Herrero-Bervera, 2007).

5.1.2. Thermomagnetic Curves

Curves for all the volcanic samples progressively demagnetized when heating, some samples showed sharp drops in magnetization in temperatures between 600° and 700°C indicative of hematite (O'Reilly, 1984). In other samples (e.g., MSM3), magnetization started to decrease around the 500°C (Figure S4a in Supporting Information S1), which may indicate the coexistence of magnetite and hematite (Dunlop & Özdemir, 1997). Some

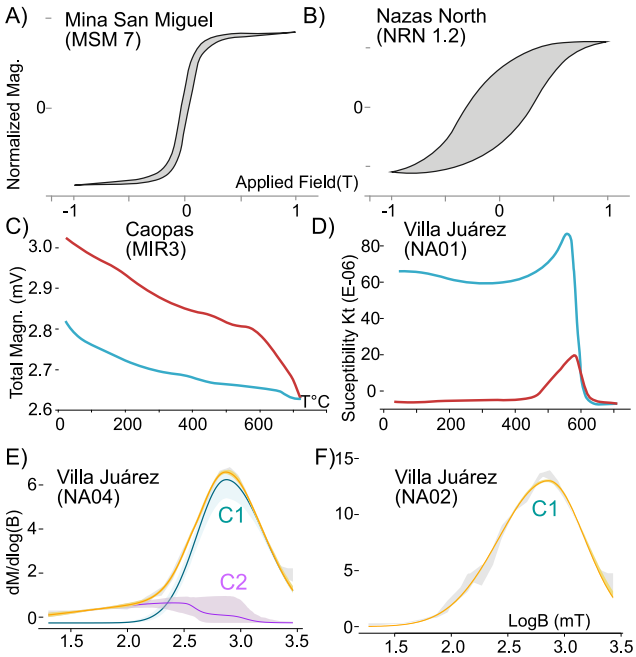

Figure 3. Rock magnetic properties graphs of representative samples. Hysteresis loops executed in magnetic field increments of 20 mT on an average time of 600 ms and corrected for paramagnetic-diamagnetic influence. The Mina San Miguel area shows a thin waist loop that we interpret as magnetite (a). The Nazas North loop (b) shows a high coercivity shape (likely hematite). (c) Total magnetization versus temperature (°C) for the Caopas laccolith showing hematite and magnetite unblocking temperatures. (d) Magnetic susceptibility (Kt) versus temperature (°C) curve for the Villa Juárez locality showing Hematite Red and blue lines represent heating and cooling, respectively. (e and f) show Gradient Acquisition plots of IRM acquisition curves of the Villa Juárez locality using MAX UnMix (Maxbauer et al., 2016). Gray dots and the yellow curve represent the smoothed IRM data and modeled coercivity distribution, respectively. Shaded areas represent 95% confidence intervals associated with each component. These plots show mid saturation (B1/2) of 1.7 for (e) and 2.85 for (f), magnetite, and hematite phases, respectively.

curves showed a subtle presence of sulfides suggested by a small magnetization increase between 400 and 500°C (e.g., De Boer & Dekkers, 1998). On all the volcanic samples we could only see a major phase with mineralogical alteration during heating, commonly hematite to maghemite due to temperature increment (Dunlop & Özdemir, 1997), and in some cases paramagnetic curves (Gubbins & Herrero-Bervera, 2007). Samples from the Caopas intrusive show analogous behavior as the volcanic samples (Figure 3c and Figure S4b in Supporting Information S1).

5.1.3. Anisotropy of Magnetic Susceptibility

AMS results for this locality show uniform mean anisotropies close to the mean (Km ≈ 592.7 × 10^{-9}) for both the Caopas and MSM areas. The anisotropy value (P) is low for the MSM area (<1.02). In contrast, the Caopas laccolith shows higher but variable values (1.032–1.343). The results for both areas show close-to-isotropic ellipsoids and no apparent deformation. The MSM locality, K_{min} axes are parallel to the poles of the lava-flow bedding resembling an antiformal structure. After unfolding, the K_{min} axes group on the vertical, following the bedding data, suggesting a pre-folding vertical fabric (Figure 4 MSM). The Caopas laccolith and the MSM areas show low anisotropy values coherent with isotropic ellipsoids (Figure S5 in Supporting Information S1). The Caopas laccolith shows a good grouping of the K_{min} axis on the vertical which is representative of an internally undeformed intrusive body that only recorded the effects of magmatic flow and gravity (Figure 4 Caopas). At the same time, the general direction of the magnetic lineation (K_{max}) corresponds to the direction of the mineral lineation (NE-SW) observed on the field (Guerra Roel, 2019).

5.1.4. Scanning Electron Microscopy

The MSM images show the presence of anhedral magnetite crystals surrounded by hematite weathering rims. Hematite is also present as a secondary mineral that fills fractures and, to a lesser extent, along the crystal cleavages of amphibole phenocrysts (Figures 5a and 5b, see also Figure S6 in Supporting Information S1).

5.1.5. Paleomagnetism

AF demagnetization was ineffective due to the presence of hematite. Upon demagnetization, we identified a Characteristic Remanent Magnetization (ChRM) with a downward inclination and westerly direction, isolated between 500 and 580°C and 40–60 mT (Figure 6). We named this component W (for west). This component was present in 12 sites of the Mina San Miguel (MSM) locality (Figure 7a1), 15 sites of the Caopas laccolith (Figure 7a2), and 7 sites of the Nazas North (Figure 7a3) in a total of 129 samples (see Table S2 in Supporting Information S1 for site level data). The W component in the MSM area shows a mean dec/inc of 285°/21° (geographic coordinates) downward and single polarity with a k of 10; K = 17.4 and A95 = 3.6 (Table 1). The VGP projection is well-rounded and the A95 value is between the maximum and minimum of the Deenen et al. (2011) envelope, suggesting that the observed distribution scatter can be explained only as a function of the PSV. The dispersion (k) at the site level ranges between 20 and 50 with MSM5 and MSM3 over 200 and MSM10 with the lowest (13) (Table S2 in Supporting Information S1). The fold test (Tauxe & Watson, 1994) shows a maximum between 1% and 31% unfolding (Figure 7a1). This negative fold test reveals that the W component in MSM is the product of a post-folding remagnetization. The paleomagnetic directions obtained from averaging all site-means and averaging all analyzed samples share a common true direction (Tauxe, 2010) and k.

The W component in the Caopas laccolith shows progressive demagnetization and high unblocking temperatures between 400° and 560°C (Figure 6 MIR-2E), and an average dec/inc 271°/18° in geographic coordinates

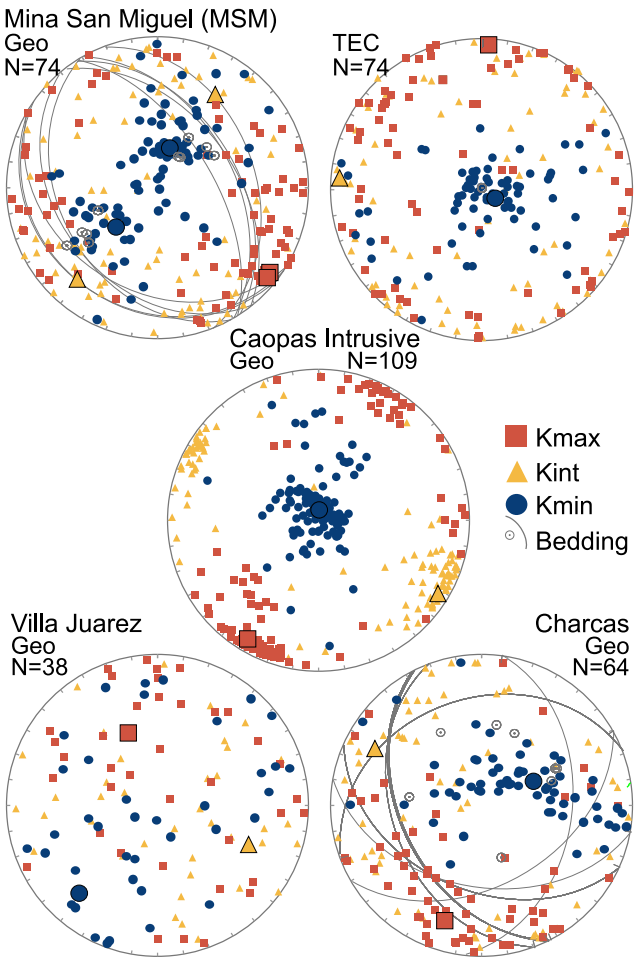

Figure 4. AMS results represented in an equal area projection for the analyzed sites in the Mina San Miguel, Villa Juárez, Charcas show results of the volcanic rocks of the Nazas Fm., and The Caopas Laccolith. Larger symbols with black outline represent site mean values. Gray lines represent bedding. Shape parameter T versus Mean magnetic susceptibility Km, and shape parameter T versus Anisotropy parameter P graphs, show low degree of anisotropy (see Figure S5 in Supporting Information S1).

(Figure 7a2) with a precision parameter k = 10. The VGPs plotted for this area have a K of 13.40 and an A95 of 5.66 in between the A95 min and A95max envelope (Table 1). The VGP plot reveals an elliptical shape, elongated W-E (Figure 7a2). Despite being within Deenen's limits, we think that the elliptical shape indicates an external cause of additional scatter apart from PSV. We suspect an unaccounted structural or magnetic acquisition problem; we will use this result with caution hereafter.

The last group of samples in the San Julián Uplift area Nazas North (Figure 6, ALI-5D; Figure 7a3) behaves similarly but with larger dispersion for the W component. This locality lies on the northern part of the San Julián Uplift and it lacks reliable structural correction due to poor exposure in the area. The mean dec/inc of the W component is 262°/27° and has a dispersion parameter k = 8.3 and A95 = 11°The Nazas North directions in this area show a large dispersion in declinations, which becomes especially obvious in the VGP projections quite elongated in the E-W coordinate (Figure 7a3). Its A95 of 11.21 is larger than Deenen's A95max, indicating additional sources of scatter not attributable to PSV. Although we cannot precisely identify the additional source of scatter, we think that it might be due to unidentified structural problems or magnetic acquisition. "Nazas North" area did not provide a data set with enough quality to quantify vertical axis rotations or latitudinal motion. However, its average declination and inclination are analogous to MSM and Caopas intrusive areas reinforcing their meaning.

5.2. Real de Catorce

5.2.1. Paleomagnetism

Samples show a single ChRM component showing a gradual demagnetization to the origin (Figure 6 RC11-A). Overall results group around two sets of directions: one with dec/inc = 358°/40° and k = 45 (K = 41, A95 = 2.79), which is similar to the Holocene GAD for Mexico; and a second one with reverse polarity dec/inc = 166°/42° and k = 41 (K = 37; A95 = 2.49). These two directions do not share a bootstrapped common true mean direction (Tauxe, 2010). However, they are not far from it, being the reversed component slightly rotated counterclockwise (<10°). The data of this locality allowed for a fold test (Tauxe & Watson, 1994) (Figure 7b). The fold test is negative with a maximum grouping between −15% and −5% unfolding. The VGPs projection shows a rounded shape (Figure 7b). By flipping the reversed directions, we obtain a mean dec/inc of 347°/43° k = 41, K = 37, A95 = 2.49 (Table 1, see also Table S3 in Supporting Information S1).

5.3. Charcas

5.3.1. Anisotropy of Magnetic Susceptibility

The magnetic susceptibility (Km) in the Charcas locality, varies from 1.209×10^{-4} to 3.353×10^{-4} with a mean value of 2.078×10^{-4} and a P = 1.24. Samples from sites CHA1, CHA2, CHA4, CHA9, and CHA10 show oblate geometries. Sites CHA3, CHA5, and CHA8 show both prolate and oblate, and CHA6 and CHA7 only show prolate geometries (Figure S5 in Supporting Information S1). K_{min} axes are parallel to the poles of the bedding except for sites CHA2, CHA3, and CHA6. AMS in Charcas seems to respond, at least partially, to loading (Figure 4 Charcas).

5.3.2. Paleomagnetism

Sites CHA1, CHA9, and CHA10 (17 samples)show a demagnetization to the origin (Figure 6 CHA-10B) with low MAD (<5). Samples from sites CHA3, 4, 5, and 6 (22 samples) show little AF demagnetization, due to the

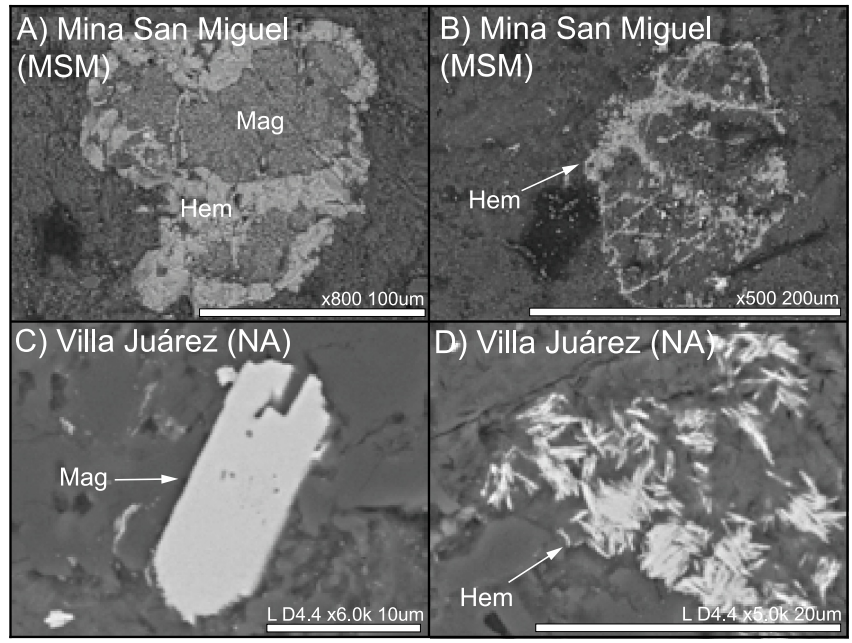

Figure 5. Scanning Electron photomicrographs of representative samples of the Nazas Fm. in the areas of Mina San Miguel and Villa Juárez. Photomicrographs of samples collected at the Mina San Miguel area show primary magnetite with alteration rims of hematite and hematite that grew in the fractures of an amphibole crystal (a and b). The Villa Juárez locality (c and d) show Fe oxides with compositions and texture of primary magnetite, Ti-magnetite, and hematite.

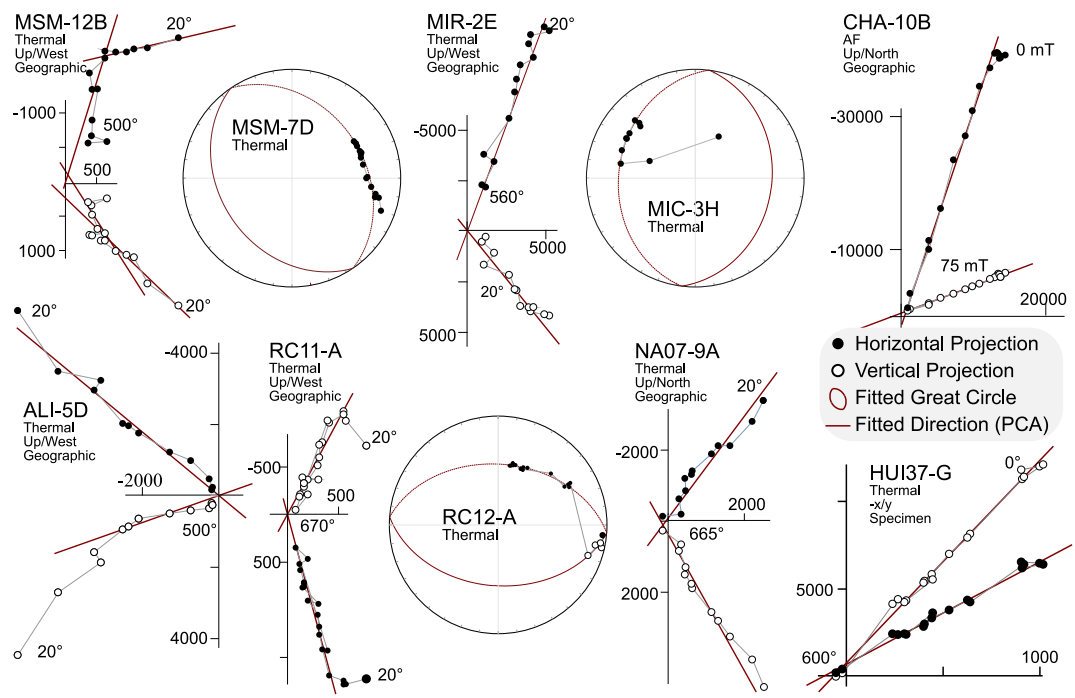

Figure 6. Directions obtained from the samples collected are expressed in Zijderveld (1967) diagrams and fitted great circles. (MSM) Mina de San Miguel locality, (MIR, MIC) Caopas Laccolith, (CHA) Charcas, (ALI) Nazas North are representative samples from the Nazas Fm. and (RC) Real de Catorce, and (HUI) Huizachal belong to the red beds formations sampled in Geographic Coordinate system. *AF* = Alternating Fields Demagnetization, *Thermal* = Thermal Demagnetization. *PC* = Principal Component.

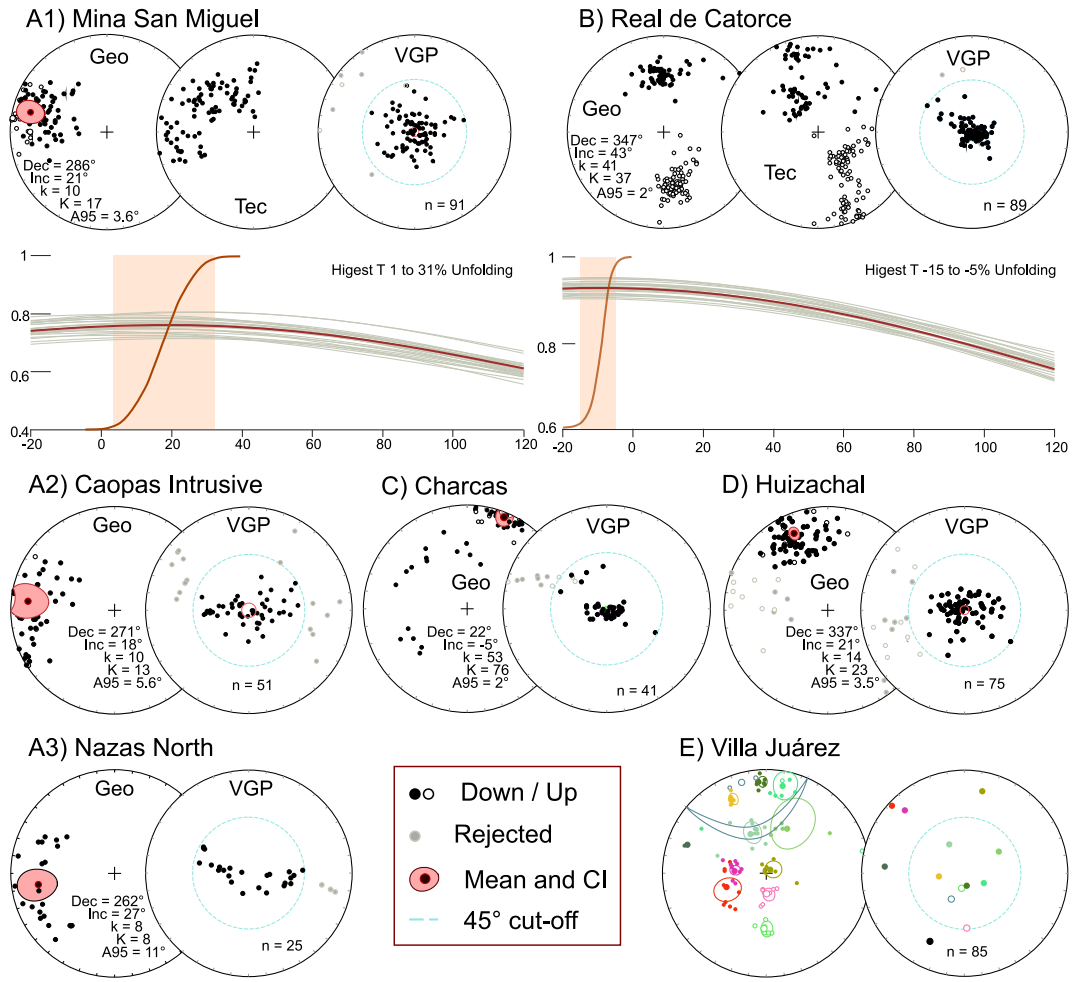

Figure 7. Equal area projections of the direction vectors of all the localities sampled in this work all shown as normal polarity but Real de Catarce that shows two polarites. Bootstrapped fold test of the Mina de San Miguel (a_1) and Real de Catorce areas (b). The projections show behavior of paleomagnetic directions during unfolding from 0% (geographic) to 100% (Tectonic; a1 and b). *Geo* = geographic; *VGP* = Virtual Geomagnetic Poles (for locality mean parameters please see Table 1).

presence of hematite, but all of them tend to the origin with analogous directions to CHA9 and CHA10. The component was isolated between 35 and 90 mT. CHA3 to CHA10 group well with a dec/inc = 22°/−05° and k = 53; K = 76; and A95 = 2.58 (Figure 7c). Samples from CHA1 and CHA2 fall out of a 45° cut-off (Figure 7c). The dispersion parameter before and after tectonic correction is k > 50 and K > 70 in both specimen and site mean averages (Table S4 in Supporting Information S1). This data suggests that sites CHA3-CHA10 may represent a single spot-reading of the geomagnetic field, either because all sample layers represent a single cooling unit or because they were quickly remagnetized later.

5.4. Huizachal Valley

5.4.1. Paleomagnetism

We identified a component isolated in the temperature range between 450 and 650°C (e.g., Figure 6 HUI47-B) combining 57 directions with 33 great circles (McFadden & McElhinny, 1988). This component has a mean dec/inc of 157°/−21° upwards with a k = 14, K = 22, and A95 = 3° (Flipped in Figure 7d and Table 1, Table S5 in Supporting Information S1). The VGPs projection shows a roughly circular shape with a slight ellipticity W-E possibly indicating tectonic-induced scatter (Figure 7d).

5.5. Villa Juárez

5.5.1. Thermomagnetic Curves

Irreversible curves are evident, and they are indicative for mineralogical alterations during heating, in most of the curves a drop in susceptibility is noticed around the Curie temperature for low Ti-magnetite (~580°C, Figure 3d), and in some cases a subtle drop around the Néel temperature (~700°C; Figure S7 in Supporting Information S1).

5.5.2. IRM

Eleven samples in the Villa Juárez locality were selected for IRM acquisition curves (NA01, NA02, NA05, and NA10 of andesitic and tuff composition along with volcano-sedimentary samples labeled NA04, NA06, NA07, NA08). The Gradient Acquisition Plots (GAP) show two components in the coercivity spectra. One with a mid-saturation value log $B_{1/2}$ between 2.85 and 3 (Figures 3e and 3f), and a second one between 1.7 and 2. Most of the results show a gradual increment toward 1 T and higher. The samples do not reach saturation at 3 T. The main contribution to the coercivity spectra is given by the log $B_{1/2}$ >100 mT and <1,000 mT. This is usually accredited to phases of hematite, which is present in both volcanic and volcano-sedimentary rocks of this locality. The remaining IRM unmixing graphs are available in Figure S8 of the Supporting Information S1.

5.5.3. Anisotropy of Magnetic Susceptibility

The mean anisotropy value (Km) varies per site from 1.95×10^{-05} to 1.59×10^{-04} with mean values of 7.36×10^{-05}. Most of the samples show oblate shapes with a low degree of anisotropy (P = 1.026; Figure S5 in Supporting Information S1). The results of the AMS ellipsoid show widespread distribution and poor grouping (Figure 4 VJ), this behavior fits well with an undeformed or faintly deformed volcanic rock, which is consistent with field observations.

5.5.4. Scanning Electron Microscopy

The SEM images were complemented with EDS scans that showed percentages of the elements present in the minerals. The images for this locality show the presence of Ti-Magnetite set in a non-conductive granular matrix (Figure 5c). Additionally, lamellar hematite crystals were observed in this locality (Figure 5d, see also Figure S6 in Supporting Information S1).

5.5.5. Paleomagnetism

The Zijderveld diagrams from this locality show a single component that progressively demagnetizes to the origin (Figure 6 NA07). The ChRM components were isolated at high temperatures (~450–700°C). At the site level, the direction means show high precision parameters in all samples but three (k > 45), whereas 5 out of 10 sites with n > 3 samples show k > 100. We consider all sites spot readings of the geomagnetic field. However, site averages do not concentrate (Figure 7e) (k < 2, without a cut-off and k = 13 after discarding more than half of site averages). Some site directions may represent reversed chrons, but our data set is too scarce to confirm. For this reason, we were not able to obtain a mean dec/inc of this locality (also see Table S6 in Supporting Information S1).

6. Timing of Magnetization

The Mesozoic and Cenozoic geological history of this Sierra Madre Oriental includes a broad spectrum of tectonic processes, including subduction, terrain accretion, large-scale deformation, and magmatism (Centeno-García, 2017; Fitz-Díaz et al., 2018; Martini & Ortega-Gutiérrez, 2018). Each of these processes may partially or completely overprint the original magnetizations of the studied rocks. In the following paragraphs, we explore the magnetization timing of our new data sets.

6.1. Primary Magnetizations

We think that the Villa Juárez locality exhibits characteristics of a primary magnetization. Each site corresponds to a single lava flow. Lava flows cool rapidly and capture snapshots of the magnetic field. Most of our sites from the Villa Juárez locality show high concentration parameters (k > 100) that are consistent with spot-readings of

the geomagnetic field (Deenen et al., 2011; Gerritsen et al., 2022; Figure 7e and Table S6 in Supporting Information S1). Some remagnetization processes could produce high concentration parameters (e.g., Pastor-Galán et al., 2021). However, they would remagnetize all lava flows as a whole in a rather small sampling area like Villa Juárez. In this locality, the average declination and inclination obtained from each lava flow differ noticeably (Figure 7e). Site averages fail to group around VGPs that resemble the GAD's PSV, despite the strong consistency within each lava flow. This peculiar result may be the consequence of a primary magnetization acquired during the 195–180 Ma lapse, when the magnetic field was unstable and reversed and excursed frequently (e.g., Ogg, 2020). In general terms, multiple spot-readings of the magnetic field spanning a sufficient period of time are required to average out paleosecular variation (PSV; Deenen et al., 2011; Gerritsen et al., 2022). Unfortunately, the studied outcrops did not include a large enough number of lava flows to average such a highly variable PSV. The data set, therefore, does not meet the current reliability criteria (e.g., Gerritsen et al., 2022; Meert et al., 2020). In this locality, we have identified magnetite and hematite as magnetic carriers (Figures 3d–3f). SEM images (Figures 5c and 5d) show a texture of well-formed euhedral to subhedral crystals of magnetite and hematite with no apparent neo-forming minerals, signs of alteration, weathering, nor apparent penetrative deformation, which supports the primary magnetization for the Villa Juárez locality. We, therefore, interpret an Early Jurassic (195 ± 7 Ma) magnetization corresponding with lava cooling (Barboza-Gudiño et al., 2021).

6.2. Late Jurassic Remagnetizations

The samples collected at three areas of the San Julián Uplift locality (Mina San Miguel, Caopas, and Nazas North) contain hematite and magnetite documented in rock magnetic analyses and SEM (Figures 3 and 5 and Figures S3, S4a, S4b, and S6 in Supporting Information S1). The ChRM (W) is carried by magnetite and yields a negative fold test (Figure 7) indicates that the MSM area was remagnetized post-folding. The similarity between the obtained directions in the three areas in geographic coordinates and the lack of observed reversals recorded in them support the idea that the areas of Caopas and Nazas N were also (re)magnetized at the same time as the MSM area. All three areas of the San Julián Uplift locality show shallow inclinations (Figure 7) that fit the expected inclination for the Late Jurassic (Vaes et al., 2023).

The timing of the folding of the anticline sampled in the MSM is unknown. Previous studies have interpreted the MSM anticline as a drape fold formed in association with a thick-skinned tectonic event. According to this interpretation, the anticline would have formed during the movement of the reverse fault that exhumed the San Julián Uplift during the Eocene (Guerra Roel, 2019; Patiño-Mendez, 2022; Ramírez-Peña & Chávez-Cabello, 2017). However, the shallow inclinations found in the MSM area in geographic coordinates are not compatible with a post-Eocene remagnetization (Figure 8). One possibility that could explain the shallow inclinations is a rapid post-Eocene remagnetization that yielded a biased shallow inclination due to insufficient PSV averaging. However, this hypothesis is weak since the VGP shape and k parameters are compatible with correct averaging of the PSV. We believe that our data aligns better with a Late Jurassic remagnetization driven by the emplacement of igneous rocks (Anderson et al., 1991; Guerra Roel, 2019; Jones et al., 1995; Ramírez-Peña, 2017; Ramírez-Peña & Chávez-Cabello, 2017).

The weakness of the Late Jurassic remagnetization hypothesis lies in the fact that nobody has suggested a Late Jurassic origin for the MSM anticline. However, the emplacement of other minor bodies associated with this Late Jurassic magmatic pulse at the Huizachal Valley (Figure 2) has been blamed for causing the angular unconformities between the members of La Boca and between La Boca and La Joya fms (Fastovsky et al., 2005; García-Obregón, 2008; Rubio-Cisneros, 2012; Rubio-Cisneros et al., 2011). We think that the emplacement of the Caopas laccolith around 165 Ma might be large enough to generate at least part of the local antiformal structure in the San Julián Uplift, in a manner similar to that described in Bunger and Cruden (2011) and Wilson et al. (2016). Subsequent cooling of the Caopas laccolith and post-emplacement fluid circulation could be the causes of the remagnetization.

We also interpret that the Huizachal locality remagnetized during the Jurassic. Its fold test (Figure S9 in Supporting Information S1) is inconclusive, and we do not have another field test to ascertain a relative timing for the magnetization in this area. Nonetheless, we found no reversals registered in the samples from this locality, which spans over 18 million years of the Jurassic (184–166 Ma). We think that a secondary magnetization for the locality can better explain our results, as the geomagnetic field during that lapse in the Jurassic was extremely variable

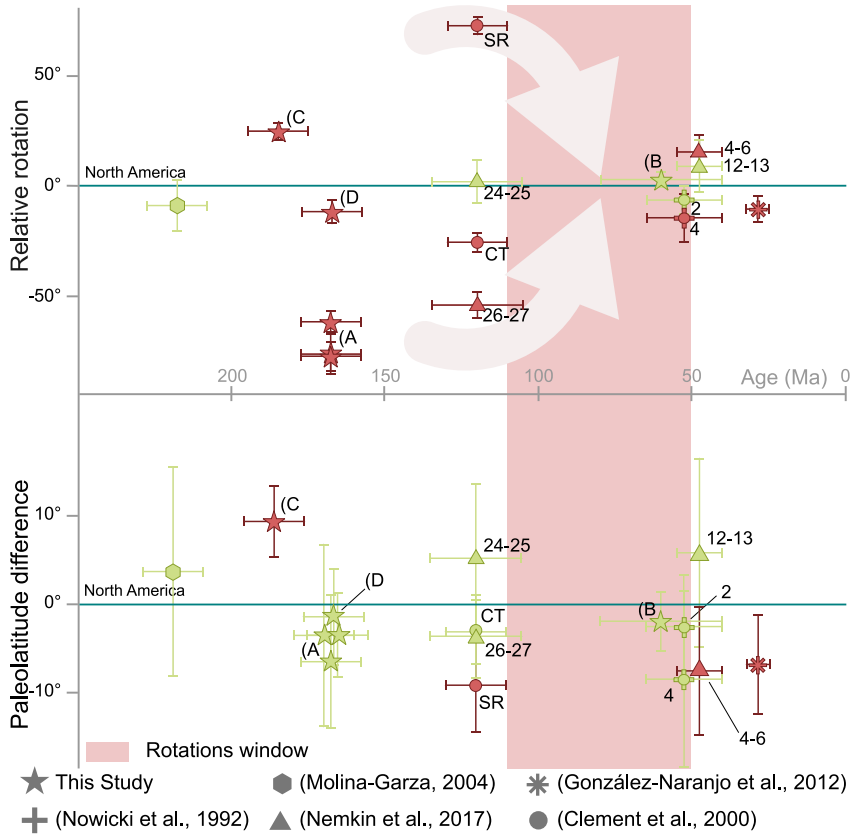

Figure 8. Observed declinations and inclinations from sampled localities and Global Apparent Wander Path of the study area for North America (Vaes et al., 2023). All localities are represented in geographic coordinates. (a) San Julián Uplift (MSM, Caopas, and Nazas North), (b) Real de Catorce, (c) Charcas, (d) Huizachal Valley. Red/Green colored directions are not/concordant with stable North America. Note that in the northern limb (CCW rotations) the localities of the San Julian Uplift area show rotations ranging ~60°–~75°, the Nem 26–27 locality ~50° and the Cle-CT with 25° all CCW rotations. In contrast, in the southern limb, Data from Charcas locality (020°/01°) shows a potential clockwise rotation of up to ~30°. Although Charcas data set may represent a single spot-reading (see Section 5.1), the rotation is large enough to infer that is significant. The locality Cle-SR show CW rotations of ~70°, this locality suffered local vertical axis rotations and therefore does not serve as a proxy for the southern limb (see Section 5.1).

(Ogg, 2020). However, the inclinations (Figure 7d), fit with a Late Jurassic remagnetization, no younger than 140 Ma, as they did in the San Julian Uplift locality.

In the Charcas locality, we found eight sites (CHA3–CHA10) that show a large directional consistency (k = 53 at specimen level; k = 87 when considering the average of the site means). Such results indicate that either CHA3 to CHA10 sites correspond with a single cooling unit or that all sites were remagnetized simultaneously (Figure 6 CHA10 and Figure 7c; Table S4 in Supporting Information S1). CHA-1 and CHA-2 sites yielded very different directions (Figure 7c). Their differences might be explained either by an extreme PSV event during acquisition (either primarily or during a remagnetization) or by two or three different magnetization events. Unfortunately, our data set is not large enough to support any of these or alternative hypotheses.

6.3. Postfolding Remagnetizations

Samples from the Real de Catorce locality show a negative fold test (Figure 7b). Folding in the Real de Catorce area has been dated to between 91 and 60 Ma (Ar-Ar in illite, Gutiérrez-Navarro et al., 2021). In contrast to the San Julián Uplift locality, the inclinations in Real de Catorce match those expected for Cretaceous and younger rocks (<140 Ma; Figure 8). The occurrence of double polarity (Figure 7b) indicates that the samples did not remagnetize, or at least not completely, during the Cretaceous superchron that ended ~83 Ma (Ogg, 2020). Hypothesizing a precise age of remagnetization is challenging but considering the post-folding and post-

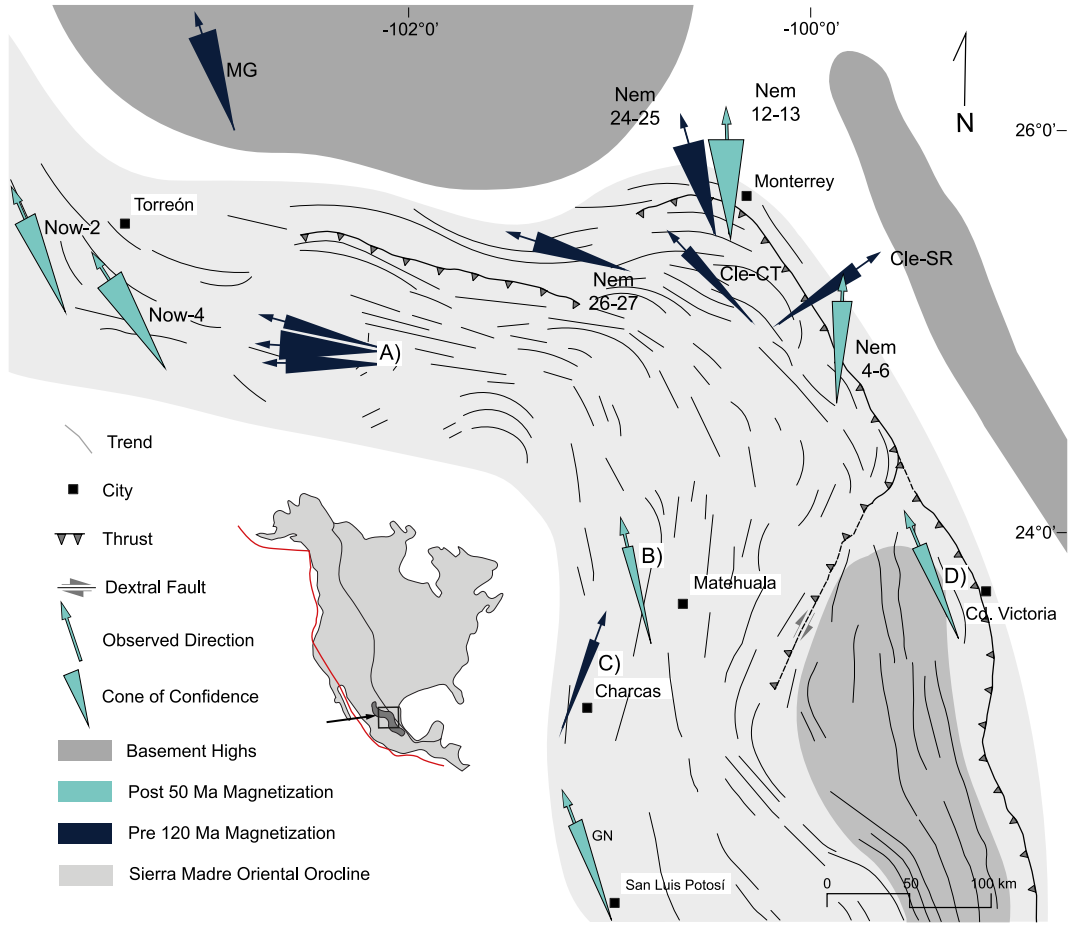

Figure 9. Schematic-structural map of the trend of the Sierra Madre Oriental Orocline. Obtained directions from this study as well as those from the revised literature. Sampled areas: (a) San Julián Uplift (MSM, Caopas and Nazas North), (b) Real de Catorce, (c) Charcas, (d) Huizachal Valley. Villa Juarez locality was excluded from any further analyses. Directions obtained from the literature (Now: Nowicki et al. (1993), MG: Molina Garza (2004), Nem: Nemkin et al. (2019), Cle: Clement et al. (2000), GN: González-Naranjo et al. (2012)).

superchron character of the magnetization, we think that a Paleocene-early Eocene remagnetization is the most likely time.

7. Vertical Axis Rotations: The Sierra Madre Oriental Orocline

The curved nature of the Sierra Madre Oriental in North Central Mexico has often been overlooked. So far, the only explanations provided consider the curvature a primary feature respect with the formation of the Mexican Fold and Thrust Belt: significant left-lateral faulting during the Late Jurassic (e.g., Anderson et al., 2005) or an inherited curvature resulting from a curved portion of the subduction zone (e.g., Molina-Garza et al., 2020).

The Triassic results from Molina Garza (2004, Figure 9), collected in an area unaffected by the deformation of the Mexican Fold and Thrust Belt, show no rotations compared to the Vaes et al. (2023) GAPWaP for North America. The new results from the Nazas, La Boca, and La Joya Formations, combined with critically reviewed data sets (Clement et al., 2000; Nemkin et al., 2019; Nowicki et al., 1993), reveal significant counterclockwise rotations in the northern limb of the study area (up to 75°) and lesser clockwise rotations in the southern limb (up to 30°) for rocks that were remagnetized before 120 Ma. Figure 8 illustrates the rotation magnitudes observed in relation to the Vaes et al. (2023) GAPWaP for North America and the inferred age of magnetization (also listed in Table 1). Rocks remagnetized during the Paleocene-early Eocene show minor rotations, most of them not significant enough (Figures 8 and 9).

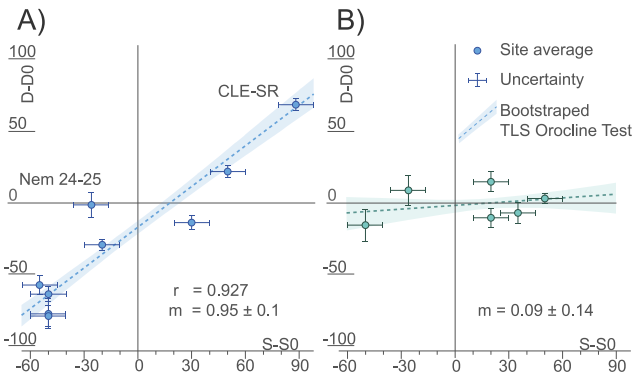

Figure 10. Bootstrapped orocline test (Pastor-Gálan et al., 2017) for pre-120 Ma directions (a) and post- 50 Ma (b). Dashed lines with shaded area represent Total Least Squares (TLS) regression and uncertainty respectably. (a) Pre- 120 ma Strike test suggests a secondary oroclinal bending/buckling. The strike of Santa Rosa locality of Clement et al. (2000) (CLE-SR) was estimated from data in Chavez-Cabello et al. (2004). Nem 24–25 seems to be an outlier, likely due to its position within the orocline hinge or unaccounted structural problems. Strike test (b) with slope of 0 suggests that the curvature of the SMO predates 50 ma.

The vertical axis rotations found in the rocks magnetized during the Jurassic and Cretaceous correlate with the changes in the trend of the regional structures (Figure 9). We hypothesize that the curvature of the Sierra Madre Oriental (Figures 2 and 9) is an orocline sensu Weil and Sussman (2004) and Pastor-Galán et al. (2017). To test the hypothesis of orocline formation, we performed two strike tests (Eldredge et al., 1985; Schwartz & Van der Voo, 1983; Yonkee & Weil, 2010), one for the rocks that magnetized before 120 Ma and another for those which did it after the Paleocene-early Eocene (Figure 10). The strike tests were performed following the methodology outlined by Pastor-Galán et al. (2017) using paleomagnetism.org software (Koymans et al., 2016, 2020). Strike tests evaluate the relationship between variations in the regional structural trend and paleomagnetic declinations, distinguishing between two endmembers: (a) a primary curve (slope m = 0), and (b) a secondary orocline (m = 1). Intermediate slopes indicates a progressive orocline. For the strike tests, we determined a regional strike for each site based on satellite images from the sampling area in combination with geological maps. The strike for the Santa Rosa Canyon (Clement et al., 2000) locality was determined following the maps and observations of Chávez-Cabello et al. (2011).

Although our strike tests do not contain enough data to be used as quantitative test (see Pastor-Galán et al., 2017 for details), our data reveals a significant correlation between strike and declinations. Altogether, the localities with pre-Cretaceous folding time (older than 120 Ma) plot a slope of 0.95 ± 0.1 (0.93 ± 0.15 if we exclude the Santa Rosa Canyon locality), indicating that the Sierra Madre Oriental was roughly linear and bent or buckled after 120 Ma (Figure 10a). The strike test for localities with Paleocene-early Eocene magnetizations shows a slope of 0.09 ± 0.14, suggesting that most vertical axis rotation associated with the curvature of the Sierra Madre Oriental had ceased after ca. 50 Ma (Figure 10b).

Following the strike test analyses, we term the curved structure of NE Mexico the "Sierra Madre Oriental Orocline." Since Cretaceous rocks holding pre-folding magnetizations (e.g., Clement et al., 2000; Nemkin et al., 2019) show the full orocline-related vertical axis rotation, we assign the age of the youngest of these rocks (120 Ma) as the maximum pre-orocline timing. Additionally, Paleocene-early Eocene magnetizations support little to no rotation, and the Eocene thick-skinned event is characterized by high-angle faults that cut across the trace of the orocline (e.g., the Norias fault that borders the San Julián Uplift "A" in Figure 2; see Guerra Roel, 2019; Ramírez-Peña & Chávez-Cabello, 2017). Therefore, we conclude that by Eocene times (ca. 50 Ma), the orocline bending/buckling had ceased. The available data set cannot provide a more precise kinematic constraint at this stage; thus, any suggestions for the mechanisms of formation or involvement of deeper lithospheric levels during the orocline formation would be highly speculative. Our data do support that the Sierra Madre Oriental Orocline developed during the Mexican orogen if we consider the timing of Guerrero Terrane accretion (Late Cenomanian, Martini et al., 2014), Arperos basin closure (Centeno-García et al., 2008), and the diachronic west to east development of the Mexican Fold Thrust belt and the thick-skinned event (90 and 42 Ma; Fitz-Díaz et al., 2018).

The occurrence of a large-scale orocline bending or buckling event in the North American Cordillera holds the potential to change our view of that complex Mesozoic-Cenozoic tectonic system. Understanding the mechanisms that formed the Sierra Madre Oriental Orocline will provide crucial information toward a detailed understanding of the Eastern Pacific-Panthalassa subduction system and its role during the break-up of Pangea. In addition, the kinematics of the Sierra Madre Oriental Orocline have the potential to unravel the tectonic evolution of the basement highs and cratonic blocks of northeast Mexico. The study of these blocks, thought to be mobile during the Mesozoic to Eocene, has been typically hampered by the lack of outcrop and scarcity of available geophysics data sets (e.g., Keppie, 2004; Lawton & Molina Garza, 2014). Further knowledge on the distribution and kinematic evolution of these terranes is not only important toward the Mesozoic and Cenozoic tectonic histories but also to understand the Paleozoic and earlier evolution of North America. We urge for more comprehensive paleomagnetic and structural data to quantitatively and effectively address this novel and captivating challenge.

8. Conclusions

- We have found significant vertical-axis rotations and a complex history of remagnetizations in the Sierra Madre Oriental.
- We documented two remagnetization events in the Sierra Madre oriental in NE Mexico: (a) a widespread Late Jurassic remagnetization that affected the Nazas, La Joya and La Boca formations, triggered by the intrusion of hypabyssal bodies. And (b) a remagnetization event that we dated in younger than 50 Ma.
- The observed rotations in the Sierra Madre Oriental imply the formation of an orocline likely occurred during the Late Cretaceous-early Eocene (120–50 Ma).
- We propose the Sierra Madre Oriental Orocline, a 450 km long and ∼110° curved mountain belt that spans from Durango to San Luis Potosí states in Northeastern Mexico.

Data Availability Statement

Raw data is available in the open-access server Zenodo.org (Guerra Roel, 2023). Paleomagnetic directions from raw and all the interpretations are stored in de data library of Paloemagnetism.org (Koymans et al., 2016, 2020) and open-source software that follows the FAIR principles, under the Persistent Identifier (PID): 26cc036dbff37a3969eaf8d25e17c2cdd2c9111165db2190efbf77d879ea7830. Raw directional data is provided in different files, all of them can be opened with Paleomagnetism.org. Collection files (.col) and comma separated values (.csv) include all metadata. Anisotropy of Magnetic Susceptibility data corresponds to AGICO "Anisoft" software version 5.1.08 available at www.AGICO.com.

Acknowledgments

We would like to thank the constructive comments of Isabelle Manighetti, Mark Dekkers and Bjarne Almqvist. The thorough and constructive comments by the three anonymous reviewers greatly improved this paper. RGR thanks the CONAHCYT for the support in the form of a doctoral scholarship, and by a Ramón y Cajal Fellow granted to DPG (RYC2019-028244-I) funded by MCIN/AEI/10.13039/501100011033 and by the "European Social Fund Investing in your future." DPG is funded by a Grant PID2021-128801NA-I00 funded by MCIN/AEI/10.13039/501100011033, a Ramón y Cajal Fellow RYC2019-028244-I funded by MCIN/AEI/10.13039/501100011033 and by the "European Social Fund Investing in your future," and a Leonardo Grant 2022 to researchers and cultural creators (LEO22-2-3010) from the bank BBVA. GCC is grateful for the support from PAICYT projects: CT1248-20, CT1626-21, and 36-CAT-2022. JJAG gratefully acknowledges PAPIIT UNAM Grants IN106820 and IG101523. GN and ARP thank the Mexican Science Agency (CONAHCYT) for the support in the form of a MSc scholarship. We appreciate the support of John W. Geissman for the access to the University of Texas paleomagnetism laboratory. A big thanks to Harald Böhnel and the guys at the Paleomagnetism laboratory in the Centro de Geociencias (CEGEO) Juriquilla for all the support and help. Part of the data sets in this paper are the late Roberto Stanley Molina Garza's unpublished work, a friend, and a mentor that will be greatly missed. RIP.

References

Abrajevitch, A. V., Ali, J. R., Aitchison, J. C., Badengzhu, Davis, A. M., Liu, J., & Ziabrev, S. V. (2005). Neotethys and the India–Asia collision: Insights from a palaeomagnetic study of the Dazhuqu ophiolite, southern Tibet. *Earth and Planetary Science Letters*, *233*(1), 87–102. https://doi.org/10.1016/j.epsl.2005.02.003

Anderson, T. H., McKee, J. W., & Jones, N. W. (1991). A northwest trending, Jurassic Fold Nappe, northernmost Zacatecas, Mexico. *Tectonics*, *10*(2), 383–401. https://doi.org/10.1029/90TC02419

Anderson, T. H., & Schmidt, V. A. (1983). The evolution of Middle America and the Gulf of Mexico–Caribbean Sea region during Mesozoic time. *Geological Society of America Bulletin*, *94*(8), 941. https://doi.org/10.1130/0016-7606(1983)94<941:TEOMAA>2.0.CO;2

Anderson, T. H., Silver, L. T., Nourse, J. A., McKee, J. W., & Steiner, M. B. (2005). *The Mojave-Sonora megashear-Field and analytical studies leading to the conception and evolution of the hypothesis* (Vol. 393, p. 1). Special Papers-Geological Society of America.

Bagheri, S., & Damani Gol, S. (2020). The eastern Iranian orocline. *Earth-Science Reviews*, *210*, 103322. https://doi.org/10.1016/j.earscirev.2020.103322

Barboza-Gudiño, J. R., Hoppe, M., Gómez-Anguiano, M., & Martínez-Macías, P. (2004). Aportaciones para la interpretación estratigráfica y estructural de la porción noroccidental de la Sierra de Catorce, San Luis Potosí, Mexico. *Revista Mexicana de Ciencias Geológicas*, *21*(3), 299–319.

Barboza-Gudiño, J. R., Molina-Garza, R. S., & Lawton, T. F. (2012). Sierra de Catorce: Remnants of the ancient western equatorial margin of Pangea in central Mexico. In J. J. Aranda-Gómez, G. Tolson, & R. S. Molina-Garza (Eds.), *The southern Cordillera and beyond* (Vol. 25, p. 0). Geological Society of America. https://doi.org/10.1130/2012.0025(01)

Barboza-Gudiño, J. R., Ocampo-Diaz, Y. Z. E., Zavala-Monsivais, A., & Lopez-Doncel, R. A. (2014). Procedencia como herramienta para la subdivision estratigrafica del Mesozoic temprano en el noreste de Mexico. *Revista Mexicana de Ciencias Geológicas*, *31*, 303–324. Scopus.

Barboza-Gudiño, J. R., Orozco-Esquivel, M. T., Gómez-Anguiano, M., & Zavala-Monsiváis, A. (2008). The Early Mesozoic volcanic arc of western North America in northeastern Mexico. *Journal of South American Earth Sciences*, *25*(1), 49–63. https://doi.org/10.1016/j.jsames.2007.08.003

Barboza-Gudiño, J. R., Zavala-Monsiváis, A., Castellanos-Rodríguez, V., Jaime-Rodríguez, D., & Almaraz-Martínez, C. (2021). Subduction-related Jurassic volcanism in the Mesa Central province and contemporary Gulf of Mexico opening. *Journal of South American Earth Sciences*, *108*, 102961. https://doi.org/10.1016/j.jsames.2020.102961

Barboza-Gudiño, J. R., Zavala-Monsiváis, A., Venegas-Rodríguez, G., & Barajas-Nigoche, L. D. (2010). Late Triassic stratigraphy and facies from northeastern Mexico: Tectonic setting and provenance. *Geosphere*, *6*(5), 621–640. https://doi.org/10.1130/GES00545.1

Bartolini, C., Lang, H., & Spell, T. (2003). Geochronology, geochemistry, and tectonic setting of the Mesozoic Nazas arc in North-Central Mexico, and its continuation to northern South America (pp. 427–461).

Bartolini, C., Wilson, J. L., & Lawton, T. F. (1999). *Mesozoic sedimentary and tectonic history of North-central Mexico*. Geological Society of America.

Belcher, R. C. (1979). *Depositional environments, paleomagnetism, and tectonic significance of Huizachal red beds (Lower Mesozoic), northeastern Mexico*. University of Texas at Austin.

Boschman, L. M., van Hinsbergen, D. J. J., Kimbrough, D. L., Langereis, C. G., & Spakman, W. (2018). The dynamic history of 220 million years of subduction below Mexico: A correlation between slab geometry and overriding plate deformation based on geology, paleomagnetism, and seismic tomography. *Geochemistry, Geophysics, Geosystems*, *19*(12), 4649–4672. https://doi.org/10.1029/2018GC007739

Bunger, A. P., & Cruden, A. R. (2011). Modeling the growth of laccoliths and large mafic sills: Role of magma body forces. *Journal of Geophysical Research*, *116*(B2), B02203. https://doi.org/10.1029/2010JB007648

Busby, C. J., & Centeno-García, E. (2022). The "Nazas Arc" is a continental rift province: Implications for Mesozoic tectonic reconstructions of the southwest Cordillera, U.S. and Mexico. *Geosphere*, *18*(2), 647–669. https://doi.org/10.1130/GES02443.1

Busby, C. J., Morris, R. A., DeBari, S. M., Medynski, S., Putirka, K., Andrews, G. D. M., et al. (2023). Geology of a large intact extensional oceanic arc crustal section with superior exposures: Cretaceous Alisitos Arc, Baja California (Mexico). *Geology of a Large Intact Extensional*

Oceanic Arc Crustal Section with Superior Exposures: Cretaceous Alisitos Arc, Baja California (Mexico), 1–107. https://doi.org/10.1130/2023.2560(01)

Butler, R. (1992). *Paleomagnetism: Magnetic domains to geologic terranes*. Blackwell Science Inc.

Carey, S. W. (1955). The orocline concept in geotectonics-Part I. In *Papers and proceedings of the royal society of Tasmania* (Vol. 89, pp. 255–288).

Centeno-García, E. (2017). Mesozoic tectono-magmatic evolution of Mexico: An overview. *Ore Geology Reviews, Metallogenic and tectono-magmatic Evolution of Mexico During the Mesozoic*, *81*, 1035–1052. https://doi.org/10.1016/j.oregeorev.2016.10.010

Centeno-García, E., Anderson, T. H., Nourse, J. A., McKee, J. W., & Steiner, M. B. (2005). Review of upper Paleozoic and lower Mesozoic stratigraphy and depositional environments, central and west Mexico: Constraints on terrane analysis and paleogeography. In *Special papers-geological society of America* (Vol. 393, p. 233).

Centeno-García, E., Guerrero-Suastegui, M., & Talavera-Mendoza, O. (2008). The Guerrero Composite Terrane of western Mexico: Collision and subsequent rifting in a supra-subduction zone. In A. E. Draut, P D. Clift, & D. W. Scholl (Eds.), *Formation and applications of the sedimentary record in arc collision zones* (Vol. 436, pp. 0–308). https://doi.org/10.1130/2008.2436(13)

Chadima, M., & Hrouda, F. (2009). *Cureval 8.0: Thermomagnetic curve browser for windows*. Agico. Inc.

Chávez-Cabello, G., Aranda-Gómez, J. J., Molina-Garza, R. S., Cossío-Torres, T., Arvizu-Gutiérrez, I. R., & González-Naranjo, G. A. (2005). La falla San Marcos: Una estructura jurásica de basamento multirreactivada del noreste de Mexico. *Boletín de La Sociedad Geológica Mexicana*, *57*(1), 27–52. https://doi.org/10.18268/bsgm2005v57n1a2

Chávez-Cabello, G., Cossío-Torres, T., & Peterson-Rodríguez, R. H. (2004). Change of the maximum principal stress during the Laramide Orogeny in the Monterrey salient, northeast Mexico. In A. J. Sussman, & A. B. Weil (Eds.), *Orogenic curvature: Integrating paleomagnetic and structural analyses* (Vol. 383, pp. 0–159). Geological Society of America. https://doi.org/10.1130/0-8137-2383-3(2004)383[145:COTMPS]2.0.CO;2

Chávez-Cabello, G., Torres-Ramos, J. A., Porras-Vazquez, N. D., Cossio-Torres, T., & Aranda-Gomez, J. J. (2011). Evolucion estructural del frente tectonico de la Sierra Madre Oriental en el Canon Santa Rosa, Linares, Nuevo. *Boletín de la Sociedad Geológica Mexicana*, *63*(2), 253–270. https://doi.org/10.18268/bsgm2011v63n2a8

Clement, B. M., Poetisi, E., Bralower, T. J., Cobabe, E., & Longoria, J. (2000). Magnetostratigraphy of mid-Cretaceous limestones from the Sierra Madre of northeastern Mexico. *Geophysical Journal International*, *143*(1), 219–229. https://doi.org/10.1046/j.1365-246X.2000.00232.x

Clemons, R. E., & McLeroy, D. F. (1965). *Resumen de la geologia de la Hoja Torreon, 13R-1 (1)*. Universidad Nacional Autonoma de Mexico. Instituto de Geologia, Carta Geologica de Mexico, Serie, 1(100,000).

De Boer, C. B., & Dekkers, M. J. (1998). Thermomagnetic behaviour of haematite and goethite as a function of grain size in various non-saturating magnetic fields. *Geophysical Journal International*, *133*(3), 541–552. https://doi.org/10.1046/j.1365-246x.1998.00522.x

DeCelles, P. G., Ducea, M. N., Kapp, P., & Zandt, G. (2009). Cyclicity in Cordilleran orogenic systems. *Nature Geoscience*, *2*(4), 251–257. Article 4. https://doi.org/10.1038/ngeo469

Deenen, M. H., Langereis, C. G., van Hinsbergen, D. J., & Biggin, A. J. (2011). Geomagnetic secular variation and the statistics of palaeomagnetic directions. *Geophysical Journal International*, *186*(2), 509–520. https://doi.org/10.1111/j.1365-246x.2011.05050.x

Dickinson, W. R., & Lawton, T. F. (2001). Carboniferous to Cretaceous assembly and fragmentation of Mexico. *Geological Society of America Bulletin*, *113*(9), 1142–1160. https://doi.org/10.1130/0016-7606(2001)113<1142:ctcaaf>2.0.co;2

Dunlop, D. J., & Özdemir, Ö. (1997). *Rock magnetism: Fundamentals and frontiers*. Cambridge University Press.

Eguiluz, S., Aranda, M., & Marrett, R. (2000). Tectónica de la Sierra Madre Oriental, Mexico. *Boletín de La Sociedad Geológica Mexicana*, *53*(1), 1–26. https://doi.org/10.18268/bsgm2000v53n1a1

Eguiluz-de Antuñano, S., Aranda-García, M., & Buitrón-Sánchez, B. E. (2014). Las formaciones Gran Tesoro y Nazas: Evolución de las secuencias Triásico Superior-Jurásico Inferior en Mexico y su significado tectogenético. *Boletín de la Sociedad Geológica Mexicana*, *66*(3), 507–539. https://doi.org/10.18268/bsgm2014v66n3a8

Eichelberger, N., & McQuarrie, N. (2015). Kinematic reconstruction of the Bolivian orocline. *Geosphere*, *11*(2), 445–462. https://doi.org/10.1130/GES01064.1

Eldredge, S., Bachtadse, V., & Van der Voo, R. (1985). Paleomagnetism and the orocline hypothesis. *Tectonophysics*, *119*(1–4), 153–179. https://doi.org/10.1016/0040-1951(85)90037-x

Fastovsky, D. E., Hermes, O. D., Strater, N. H., Bowring, S. A., Clark, J. M., Montellano, M., & Rene, H. R. (2005). Pre–Late Jurassic, fossil-bearing volcanic and sedimentary red beds of Huizachal Canyon, Tamaulipas, Mexico.

Fisher, R. A. (1953). Dispersion on a sphere. *Proceedings of the Royal Society of London. Series A. Mathematical and Physical Sciences*, *217*(1130), 295–305. https://doi.org/10.1098/rspa.1953.0064

Fitz-Díaz, E., Hall, C., & Van der Pluijm, B. A. (2016). XRD-based $^{40}Ar/^{39}Ar$ age correction for fine-grained illite, with application to folded carbonates in the Monterrey Salient (northern Mexico). *Geochimica et Cosmochimica Acta*, *181*, 201–216. https://doi.org/10.1016/j.gca.2016.02.004

Fitz-Díaz, E., Lawton, T. F., Juárez-Arriaga, E., & Chávez-Cabello, G. (2018). The Cretaceous-Paleogene Mexican orogen: Structure, basin development, magmatism and tectonics. *Earth-Science Reviews*, *183*, 56–84. https://doi.org/10.1016/j.earscirev.2017.03.002

Flinn, D. (1962). On folding during three-dimensional progressive deformation. *Quarterly Journal of the Geological Society*, *118*(1–4), 385–428. https://doi.org/10.1144/gsjgs.118.1.0385

García-Obregón, R. (2008). *Cartografía geológica y petrología del vulcanismo mesozoico en el Valle de Huizachal, Tamaulipas. [Tesis de Licenciatura]*. Universidad Autónoma de Nuevo León.

Gerritsen, D., Vaes, B., & van Hinsbergen, D. J. (2022). Influence of data filters on the position and precision of paleomagnetic poles: What is the optimal sampling strategy? *Geochemistry, Geophysics, Geosystems*, *23*(4), e2021GC010269. https://doi.org/10.1029/2021gc010269

Godínez-Urban, A., Lawton, T. F., Molina Garza, R. S., Iriondo, A., Weber, B., & López-Martínez, M. (2011). Jurassic volcanic and sedimentary rocks of the La Silla and Todos Santos Formations, Chiapas: Record of Nazas arc magmatism and rift-basin formation prior to opening of the Gulf of Mexico. *Geosphere*, *7*(1), 121–144. https://doi.org/10.1130/ges00599.1

Goldhammer, R. K. (1999). Mesozoic sequence stratigraphy and paleogeographic evolution of northeast Mexico. In *Special Paper 340: Mesozoic sedimentary and tectonic history of north-central Mexico* (pp. 1–58). https://doi.org/10.1130/0-8137-2340-x.1

González-León, C. M., Vázquez-Salazar, M., Navarro, T. S., Solari, L. A., Nourse, J. A., Del Rio-Salas, R., et al. (2021). Geology and geochronology of the Jurassic magmatic arc in the Magdalena quadrangle, north-central Sonora, Mexico. *Journal of South American Earth Sciences*, *108*, 103055. https://doi.org/10.1016/j.jsames.2020.103055

González-Naranjo, G., Molina Garza, R., Aranda-Gomez, J., González, M., Aguillón-Robles, A., Iriondo, A., & Bellon, H. (2012). Paleomagnetismo y edad de la Ignimbrita Panalillo Superior, Campo Volcánico de San Luis Potosí, Mexico. *Boletin de La Sociedad Geologica Mexicana*, *64*(3), 387–409. https://doi.org/10.18268/BSGM2012v64n3a9

Gose, W. A., Belcher, R. C., & Scott, G. R. (1982). Paleomagnetic results from northeastern Mexico: Evidence for large Mesozoic rotations. *Geology*, *10*(1), 50–54. https://doi.org/10.1130/0091-7613(1982)10<50:PRFNME>2.0.CO;2

Gray, G. G., & Lawton, T. F. (2011). New constraints on timing of Hidalgoan (Laramide) deformation in the Parras and La Popa basins, NE Mexico. *Boletín de La Sociedad Geológica Mexicana*, *63*(2), 333–343. https://doi.org/10.18268/bsgm2011v63n2a13

Gubbins, D., & Herrero-Bervera, E. (2007). *Encyclopedia of geomagnetism and paleomagnetism*. Springer Science & Business Media.

Guerra Roel, R. (2019). Análisis estructural de la zona norte del bloque de San Julián, Zacatecas Mexico [Masters, Universidad Autónoma de Nuevo León]. Retrieved from http://eprints.uanl.mx/18367/

Guerra Roel, R. (2023). Repository files to "The Sierra Madre Oriental Orocline. Paleomagnetism of The Nazas province in NE Mexico [Dataset]. *Zenodo*. https://doi.org/10.5281/zenodo.10914408

Gutiérrez-Alonso, G., Fernández-Suárez, J., & Weil, A. B. (2004). Orocline triggered lithospheric delamination. In *Special paper 383: Orogenic curvature: Integrating paleomagnetic and structural analyses* (Vol. 383, pp. 121–130). Geological Society of America. https://doi.org/10.1130/0-8137-2383-3(2004)383[121:OTLD]2.0.CO;2

Gutiérrez-Alonso, G., Fernández-Suárez, J., Weil, A. B., Brendan Murphy, J., Damian Nance, R., Corfú, F., & Johnston, S. T. (2008). Self-subduction of the Pangaean global plate. *Nature Geoscience*, *1*(8), 549–553. Article 8. https://doi.org/10.1038/ngeo250

Gutiérrez-Navarro, R., Fitz Diaz, E., Barboza-Gudiño, J., & Stockli, D. (2021). Shortening and exhumation of Sierra de Catorce in northeastern Mexico, in light of $^{40}Ar/^{39}Ar$ illite dating and U–Th/He zircon thermochronology. *Journal of South American Earth Sciences*, *111*, 103334. https://doi.org/10.1016/j.jsames.2021.103334

Hernández-Romano, U., Aguilera-Franco, N., Martínez-Medrano, M., & Barceló-Duarte, J. (1997). Guerrero-Morelos platform drowning at the Cenomanian–Turonian boundary, Huitziltepec area, Guerrero State, southern Mexico. *Cretaceous Research*, *18*(5), 661–686. https://doi.org/10.1006/cres.1997.0078

Hindle, D., & Burkhard, M. (1999). Strain, displacement and rotation associated with the formation of curvature in fold belts; the example of the Jura arc. *Journal of Structural Geology*, *21*(8), 1089–1101. https://doi.org/10.1016/S0191-8141(99)00021-8

Imlay, R. W., Cepeda, E., Alvarez, M., & Diaz, T. (1948). Stratigraphic relations of certain Jurassic formations in eastern Mexico. *AAPG Bulletin*, *32*(9), 1750–1761. https://doi.org/10.1306/3d933c1d-16b1-11d7-8645000102c1865d

INEGI. (2023). *Biblioteca digital de Mapas*. Instituto Nacional de Estadística y Geografía. INEGI. Retrieved from https://www.inegi.org.mx/app/mapas/

Jelinek, V. (1981). Characterization of the magnetic fabric of rocks. *Tectonophysics*, *79*(3–4), T63–T67. https://doi.org/10.1016/0040-1951(81)90110-4

Jiménez, G., Speranza, F., Faccenna, C., Bayona, G., & Mora, A. (2014). Paleomagnetism and magnetic fabric of the eastern Cordillera of Colombia: Evidence for oblique convergence and nonrotational reactivation of a Mesozoic intracontinental rift. *Tectonics*, *33*(11), 2233–2260. https://doi.org/10.1002/2014TC003532

Johnston, S. T. (2001). The Great Alaskan Terrane Wreck: Reconciliation of paleomagnetic and geological data in the northern Cordillera. *Earth and Planetary Science Letters*, *193*(3), 259–272. https://doi.org/10.1016/S0012-821X(01)00516-7

Johnston, S. T., Weil, A. B., & Gutiérrez-Alonso, G. (2013). Oroclines: Thick and thin. *GSA Bulletin*, *125*(5–6), 643–663. https://doi.org/10.1130/B30765.1

Jones, N. W., McKee, J. W., Anderson, T. H., & Silver, L. T. (1995). Jurassic volcanic rocks in northeastern Mexico: A possible remnant of a Cordilleran magmatic arc. In C. Jacques-Ayala, C. M. González-Léon, & J. Roldán-Quintana (Eds.), *Studies on the Mesozoic of Sonora and adjacent areas* (Vol. 301, pp. 0–190). Geological Society of America. https://doi.org/10.1130/0-8137-2301-9.179

Keppie, J. D. (2004). Terranes of Mexico revisited: A 1.3 billion year Odyssey. *International Geology Review*, *46*(9), 765–794. https://doi.org/10.2747/0020-6814.46.9.765

Kirschvink, J. L. (1980). The least-squares line and plane and the analysis of palaeomagnetic data. *Geophysical Journal International*, *62*(3), 699–718. https://doi.org/10.1111/j.1365-246x.1980.tb02601.x

Kleist, R., Hall, S. A., & Evans, I. (1984). A paleomagnetic study of the Lower Cretaceous Cupido Limestone, northeast Mexico: Evidence for local rotation within the Sierra Madre Oriental. *GSA Bulletin*, *95*(1), 55–60. https://doi.org/10.1130/0016-7606(1984)95<55:APSOTL>2.0.CO;2

Kollmeier, J. M., van der Pluijm, B. A., & Van der Voo, R. (2000). Analysis of Variscan dynamics; early bending of the Cantabria–Asturias Arc, northern Spain. *Earth and Planetary Science Letters*, *181*(1), 203–216. https://doi.org/10.1016/S0012-821X(00)00203-X

Koymans, M. R., Langereis, C. G., Pastor-Galán, D., & van Hinsbergen, D. J. (2016). *Paleomagnetism. org: An online multi-platform open source environment for paleomagnetic data analysis*. Elsevier.

Koymans, M. R., van Hinsbergen, D. J. J., Pastor-Galán, D., Vaes, B., & Langereis, C. G. (2020). Towards FAIR paleomagnetic data management through Paleomagnetism. Org 2.0. *Geochemistry, Geophysics, Geosystems*, *21*(2), e2019GC008838. https://doi.org/10.1029/2019gc008838

Kruiver, P. P., Dekkers, M. J., & Heslop, D. (2001). Quantification of magnetic coercivity components by the analysis of acquisition curves of isothermal remanent magnetisation. *Earth and Planetary Science Letters*, *189*(3–4), 269–276. https://doi.org/10.1016/s0012-821x(01)00367-3

Lawton, T. F., & Molina Garza, R. S. (2014). U-Pb geochronology of the type Nazas Fm. and superjacent strata, northeastern Durango, Mexico: Implications of a Jurassic age for continental-arc magmatism in north-central Mexico. *GSA Bulletin*, *126*(9–10), 1181–1199. https://doi.org/10.1130/B30827.1

Li, P., Rosenbaum, G., & Donchak, P. J. (2012). Structural evolution of the Texas Orocline, eastern Australia. *Gondwana Research*, *22*(1), 279–289. https://doi.org/10.1016/j.gr.2011.09.009

Li, P., Sun, M., Narantsetseg, T., Jourdan, F., Hu, W., & Yuan, C. (2021). First structural observation around the hinge of the Mongolian Orocline (Central Asia): Implications for the geodynamics of oroclinal bending and the evolution of the Mongol-Okhotsk Ocean. *GSA Bulletin*, *134*(7–8), 1994–2006. https://doi.org/10.1130/B36200.1

Liu, Y., Xiao, W., Ma, Y., Li, S., Peskov, A. Y., Chen, Z., et al. (2023). Oroclines in the central Asian orogenic belt. *National Science Review*, *10*(2), nwac243. https://doi.org/10.1093/nsr/nwac243

López-Infanzón, M. L. (1986). Estudio Petrogenetico De Las Rocas Igneas En Las Formaciones Huizachal Y Nazas. *Boletín de La Sociedad Geológica Mexicana*, *47*(2), 1–41. https://doi.org/10.18268/bsgm1986v47n2a1

Maffione, M., Speranza, F., Faccenna, C., & Rossello, E. (2010). Paleomagnetic evidence for a pre-early Eocene (~50Ma) bending of the Patagonian orocline (Tierra del Fuego, Argentina): Paleogeographic and tectonic implications. *Earth and Planetary Science Letters*, *289*(1), 273–286. https://doi.org/10.1016/j.epsl.2009.11.015

Marshak, S. (1988). Kinematics of orocline and arc formation in thin-skinned orogens. *Tectonics*, *7*(1), 73–86. https://doi.org/10.1029/TC007i001p00073

Marshak, S. (2004a). *Essentials of geology*. WW Norton.

Marshak, S. (2004b). Salients, recesses, arcs, oroclines, and syntaxes—A review of ideas concerning the formation of map-view curves in fold-thrust belts. In K. R. McClay (Ed.), *Thrust tectonics and hydrocarbon systems* (Vol. 82, p. 0). American Association of Petroleum Geologists. https://doi.org/10.1306/M82813C9

Martini, M., & Ortega-Gutiérrez, F. (2018). Tectono-stratigraphic evolution of eastern Mexico during the break-up of Pangea: A review. *Earth-Science Reviews*, *183*, 38–55. https://doi.org/10.1016/j.earscirev.2016.06.013

Martini, M., Solari, L., & López-Martínez, M. (2014). Correlating the Arperos Basin from Guanajuato, central Mexico, to Santo Tomás, southern Mexico: Implications for the paleogeography and origin of the Guerrero terrane. *Geosphere*, *10*(6), 1385–1401. https://doi.org/10.1130/GES01055.1

Mauel, D. J., Lawton, T. F., González-León, C., Iriondo, A., & Amato, J. M. (2011). Stratigraphy and age of Upper Jurassic strata in north-central Sonora, Mexico: Southwestern Laurentian record of crustal extension and tectonic transition. *Geosphere*, *7*(2), 390–414. https://doi.org/10.1130/GES00600.1

Maxbauer, D. P., Feinberg, J. M., & Fox, D. L. (2016). MAX UnMix: A web application for unmixing magnetic coercivity distributions. *Computers & Geosciences*, *95*, 140–145. https://doi.org/10.1016/j.cageo.2016.07.009

McElhinny, M. W., & McFadden, P. L. (1999). *Paleomagnetism: Continents and oceans*. Elsevier.

McFadden, P. L., & McElhinny, M. W. (1988). The combined analysis of remagnetization circles and direct observations in palaeomagnetism. *Earth and Planetary Science Letters*, *87*(1), 161–172. https://doi.org/10.1016/0012-821X(88)90072-6

Meert, J. G., Pivarunas, A. F., Evans, D. A. D., Pisarevsky, S. A., Pesonen, L. J., Li, Z.-X., et al. (2020). The magnificent seven: A proposal for modest revision of the Van der Voo (1990) quality index. *Tectonophysics*, *790*, 228549. https://doi.org/10.1016/j.tecto.2020.228549

Mixon, R. B., Murray, G. E., & Teodoro, D. G. (1959). Age and correlation of Huizachal group (Mesozoic), State of Tamaulipas, Mexico: ADDENDUM. *AAPG Bulletin*, *43*(4), 757–771. https://doi.org/10.1306/0BDA5ED3-16BD-11D7-8645000102C1865D

Molina Garza, R. (2004). Paleomagnetic reconstruction of Coahuila, Mexico: The Late Triassic Acatita intrusives. *Geofísica Internacional*, *44*(2), 197–210. https://doi.org/10.22201/igeof.00167169p.2005.44.2.254

Molina-Garza, R. S., & Iriondo, A. (2005). La Megacizalla Mojave-Sonora: La hipótesis, la controversia y el estado actual de conocimiento. *Boletín de la Sociedad Geológica Mexicana*, *57*(1), 1–26. https://doi.org/10.18268/bsgm2005v57n1a1

Molina-Garza, R. S., Pindell, J., & Montaño Cortés, P. C. (2020). Slab flattening and tractional coupling drove Neogene clockwise rotation of Chiapas Massif, Mexico: Paleomagnetism of the Eocene El Bosque formation. *Journal of South American Earth Sciences*, *104*, 102932. https://doi.org/10.1016/j.jsames.2020.102932

Montes, C., Bayona, G., Cardona, A., Buchs, D. M., Silva, C. A., Morón, S., et al. (2012). Arc-continent collision and orocline formation: Closing of the Central American seaway. *Journal of Geophysical Research*, *117*(B4), B04105. https://doi.org/10.1029/2011JB008959

Nemkin, S. R., Chávez-Cabello, G., Fitz-Díaz, E., van der Pluijm, B., & Van der Voo, R. (2019). Concurrence of folding and remagnetization events in the Monterrey Salient (NE Mexico). *Tectonophysics*, *760*, 58–68. https://doi.org/10.1016/j.tecto.2017.12.002

Nowicki, M. J., Hall, S. A., & Evans, I. (1993). Palaeomagnetic evidence for local and regional post-Eocene rotations in northern Mexico. *Geophysical Journal International*, *114*(1), 63–75. https://doi.org/10.1111/j.1365-246X.1993.tb01466.x

Ocampo-Díaz, Y. Z. E., Pinzon-Sotelo, M. P., Chávez-Cabello, G., Ramírez-Díaz, A., Martínez-Paco, M., Velasco-Tapia, F., et al. (2016). Propuesta nomenclatural y análisis de procedencia de la Formación Concepción del Oro (antes Formación Caracol): Implicaciones sobre la evolución tectónica del sur de Norteamérica durante el Cretácico Tardío. *Revista Mexicana de Ciencias Geológicas*, *33*(1), 3–33.

Ogg, J. G. (2020). Chapter 5—Geomagnetic polarity time scale. In F. M. Gradstein, J. G. Ogg, M. D. Schmitz, & G. M. Ogg (Eds.), *Geologic time scale 2020* (pp. 159–192). Elsevier. https://doi.org/10.1016/B978-0-12-824360-2.00005-X

O'Reilly, W. (1984). Applications of rock and mineral magnetism. In W. O'Reilly (Ed.), *Rock and mineral magnetism* (pp. 194–212). Springer US. https://doi.org/10.1007/978-1-4684-8468-7_9

Padilla y Sánchez, R. J. (1985). Las estructuras de la Curvatura de Monterrey, estados de Coahuila, Nuevo León, Zacatecas y San Luis Potosí. *Revista Mexicana de Ciencias Geológicas*, *6*(1), 1–20.

Pantoja-Alor, J. (1972). Datos geológicos y estratigráficos de la Formación Nazas (memoria), II Convención Nacional. Mazatlán, Sinaloa, Sociedad Geológica Mexicana, 25–31.

Parés, J. M. (2015). Sixty years of anisotropy of magnetic susceptibility in deformed sedimentary rocks. *Frontiers in Earth Science*, *3*. https://doi.org/10.3389/feart.2015.00004

Pastor-Galán, D. (2022). From supercontinent to superplate: Late Paleozoic Pangea's inner deformation suggests it was a short-lived superplate. *Earth-Science Reviews*, *226*, 103918. https://doi.org/10.1016/j.earscirev.2022.103918

Pastor-Galán, D., Groenewegen, T., Brouwer, D., Krijgsman, W., & Dekkers, M. J. (2015). One or two oroclines in the Variscan orogen of Iberia? Implications for Pangea amalgamation. *Geology*, *43*(6), 527–530. https://doi.org/10.1130/G36701.1

Pastor-Galán, D., Gutiérrez-Alonso, G., Dekkers, M. J., & Langereis, C. G. (2017). Paleomagnetism in Extremadura (Central Iberian zone, Spain) Paleozoic rocks: Extensive remagnetizations and further constraints on the extent of the Cantabrian orocline. *Journal of Iberian Geology*, *43*(4), 583–600. https://doi.org/10.1007/s41513-017-0039-x

Pastor-Galán, D., Gutiérrez-Alonso, G., & Weil, A. B. (2011). Orocline timing through joint analysis: Insights from the Ibero-Armorican Arc. *Tectonophysics*, *507*(1), 31–46. https://doi.org/10.1016/j.tecto.2011.05.005

Pastor-Galán, D., Gutiérrez-Alonso, G., & Weil, A. B. (2020). The enigmatic curvature of Central Iberia and its puzzling kinematics. *Solid Earth*, *11*(4), 1247–1273. https://doi.org/10.5194/se-11-1247-2020

Pastor-Galán, D., Gutiérrez-Alonso, G., Zulauf, G., & Zanella, F. (2012). Analogue modeling of lithospheric-scale orocline buckling: Constraints on the evolution of the Iberian-Armorican Arc. *GSA Bulletin*, *124*(7–8), 1293–1309. https://doi.org/10.1130/B30640.1

Pastor-Galán, D., Martín-Merino, G., & Corrochano, D. (2014). Timing and structural evolution in the limb of an orocline: The Pisuerga–Carrión Unit (southern limb of the Cantabrian Orocline, NW Spain). *Tectonophysics*, *622*, 110–121. https://doi.org/10.1016/j.tecto.2014.03.004

Pastor-Galán, D., Pueyo, E. L., Diederen, M., García-Lasanta, C., & Langereis, C. G. (2018). Late Paleozoic Iberian orocline(s) and the missing shortening in the core of Pangea. Paleomagnetism from the Iberian Range. *Tectonics*, *37*(10), 3877–3892. https://doi.org/10.1029/2018TC004978

Pastor-Galán, D., Spencer, C. J., Furukawa, T., & Tsujimori, T. (2021). Evidence for crustal removal, tectonic erosion and flare-ups from the Japanese evolving forearc sediment provenance. *Earth and Planetary Science Letters*, *564*, 116893. https://doi.org/10.1016/j.epsl.2021.116893

Patiño-Mendez, G. (2022). *Analisis de la anisotropuia magnetica del pliegue de San Miguel. [Batchelor tesis]*. Universidad Autónoma de Nuevo León.

Pindell, J., & Kennan, L. (2001). Kinematic evolution of the Gulf of Mexico and Caribbean. In R. H. Fillon, N. C. Rosen, P. Weimer, A. Lowrie, H. Pettingill, R. L. Phair, et al. (Eds.), *Petroleum systems of deep-water basins–global and Gulf of Mexico experience* (Vol. 21, pp. 0–220). SEPM Society for Sedimentary Geology. https://doi.org/10.5724/gcs.01.21.0193

Ramírez-Peña, C. F. (2017). *Análisis de la deformación progresiva en la zona sur del sector transversal de Parras y la Saliente de Monterrey, Mexico Unpublished PhD. Tesis*. Universidad Autónoma de Nuevo León, Facultad de Ciencias de la Tierra. Retrieved from https://scholar.google.com/citations?view_op=view_citation&hl=es&user=96g7lyEAAAAJ&citation_for_view=96g7lyEAAAAJ:9yKSN-GCB0IC

Ramírez-Peña, C. F., & Chávez-Cabello, G. (2017). Age and evolution of thin-skinned deformation in Zacatecas, Mexico: Sevier orogeny evidence in the Mexican Fold-Thrust Belt. *Journal of South American Earth Sciences*, *76*, 101–114. https://doi.org/10.1016/j.jsames.2017.01.007

Ramírez-Peña, C. F., Chávez-Cabello, G., Fitz-Díaz, E., Aranda-Gómez, J. J., & Valdés, R. S. (2019). Uplift and syn-orogenic magmatism in the Concepción del Oro Block: A thick-skinned (Laramide style?) contractional structure in the Mexican Fold-Thrust Belt. *Journal of South American Earth Sciences*, *93*, 242–252. https://doi.org/10.1016/j.jsames.2019.04.012

Rezaeian, M., Kuijper, C. B., van der Boon, A., Pastor-Galán, D., Cotton, L. J., Langereis, C. G., & Krijgsman, W. (2020). Post-Eocene coupled oroclines in the Talesh (NW Iran): Paleomagnetic constraints. *Tectonophysics*, *786*, 228459. https://doi.org/10.1016/j.tecto.2020.228459

Rubio-Cisneros, I. I. (2012). Análisis de procedencia de las formaciones el Alamar, La Boca y La Joya Noreste de Mexico (triásico superior-jurásico medio) [Phd, Universidad Autónoma de Nuevo León]. http://eprints.uanl.mx/3223/

Rubio-Cisneros, I. I., & Lawton, T. F. (2011). Detrital zircon U-Pb ages of sandstones in continental red beds at Valle de Huizachal, Tamaulipas, NE Mexico: Record of Early-Middle Jurassic arc volcanism and transition to crustal extension. *Geosphere*, *7*(1), 159–170. https://doi.org/10.1130/GES00567.1

Rubio-Cisneros, I. I., Ramírez-Fernández, J. A., & García-Obregón, R. (2011). Análisis preliminar de procedencia de rocas clásticas jurásicas del valle de Huizachal, Sierra Madre Oriental: Influencia del vulcanismo sinsedimentario y el basamento cristalino. *Boletín de la Sociedad Geológica Mexicana*, *63*(2), 137–156. https://doi.org/10.18268/BSGM2011v63n2a1

Salvador, A. (1987). Late Triassic-Jurassic paleogeography and origin of Gulf of Mexico Basin1. *AAPG Bulletin*, *71*(4), 419–451. https://doi.org/10.1306/94886EC5-1704-11D7-8645000102C1865D

Sapienza, F., Gallo, L. C., Zhang, Y., Vaes, B., Domeier, M., & Swanson-Hysell, N. L. (2023). Quantitative analysis of paleomagnetic sampling strategies. *Journal of Geophysical Research: Solid Earth*, *128*(11), e2023JB027211. https://doi.org/10.1029/2023JB027211

Schwartz, S. Y., & Van der Voo, R. (1983). Paleomagnetic evaluation of the orocline hypothesis in the central and southern Appalachians. *Geophysical Research Letters*, *10*(7), 505–508. https://doi.org/10.1029/GL010i007p00505

SGM. (2023). Cartas impresas disponibles del Servicio Geológico Mexicano. Retrieved from https://www.sgm.gob.mx/CartasDisponibles/

Shaanan, U., Rosenbaum, G., Li, P., & Vasconcelos, P. (2014). Structural evolution of the early Permian Nambucca Block (New England Orogen, eastern Australia) and implications for oroclinal bending. *Tectonics*, *33*(7), 1425–1443. https://doi.org/10.1002/2013TC003426

Shaw, J., Johnston, S. T., Gutiérrez-Alonso, G., & Weil, A. B. (2012). Oroclines of the Variscan orogen of Iberia: Paleocurrent analysis and paleogeographic implications. *Earth and Planetary Science Letters*, *329*(330), 60–70. https://doi.org/10.1016/j.epsl.2012.02.014

Silva-Romo, G., Arellano-Gil, J., Mendoza-Rosales, C., & Nieto-Obregón, J. (2000). A submarine fan in the Mesa Central, Mexico. *Journal of South American Earth Sciences*, *13*(4–5), 429–442. https://doi.org/10.1016/s0895-9811(00)00034-1

Silver, L. T., & Anderson, T. H. (1974). Possible left-lateral early to middle Mesozoic disruption of the south-western North American craton margin. *Geological Society of America Abstracts and Programs*, *6*, 955–956.

Stern, R. J., & Dickinson, W. R. (2010). The Gulf of Mexico is a Jurassic backarc basin. *Geosphere*, *6*(6), 739–754. https://doi.org/10.1130/GES00585.1

Sussman, A. J., & Weil, A. B. (2004). *Orogenic curvature: Integrating paleomagnetic and structural analyses*. Geological Society of America.

Tarling, D., & Hrouda, F. (1993). *Magnetic anisotropy of rocks*. Springer Science & Business Media.

Tauxe, L. (2010). *Essentials of paleomagnetism*. University of California Press.

Tauxe, L., & Watson, G. S. (1994). The fold test: An Eigen analysis approach. *Earth and Planetary Science Letters*, *122*(3), 331–341. https://doi.org/10.1016/0012-821X(94)90006-X

Vaes, B., van Hinsbergen, D. J. J., van de Lagemaat, S. H. A., van der Wiel, E., Lom, N., Advokaat, E. L., et al. (2023). A global apparent polar wander path for the last 320 Ma calculated from site-level paleomagnetic data. *Earth-Science Reviews*, *245*, 104547. https://doi.org/10.1016/j.earscirev.2023.104547

Warrior, S. (2008). *A paleomagnetic investigation of the Mojave-Sonora megashear hypothesis in north-central and northeastern Mexico* (pp. 1–188). ETD Collection for University of Texas.

Weil, A. B., Gutiérrez-Alonso, G., & Wicks, D. (2013). Investigating the kinematics of local thrust sheet rotation in the limb of an orocline: A paleomagnetic and structural analysis of the Esla tectonic unit, Cantabrian–Asturian Arc, NW Iberia. *International Journal of Earth Sciences*, *102*(1), 43–60. https://doi.org/10.1007/s00531-012-0790-3

Weil, A. B., & Sussman, A. J. (2004). Classifying curved orogens based on timing relationships between structural development and vertical-axis rotations. In A. J. Sussman, & A. B. Weil (Eds.), *Orogenic curvature: Integrating paleomagnetic and structural analyses* (Vol. 383, pp. 1–15). Geological Society of America Special Paper. https://doi.org/10.1130/0-8137-2383-3(2004)383[1:ccobot]2.0.co;2

Weil, A. B., Van der Voo, R., & van der Pluijm, B. A. (2001). Oroclinal bending and evidence against the Pangea megashear: The Cantabria-Asturias arc (northern Spain). *Geology*, *29*(11), 991–994. https://doi.org/10.1130/0091-7613(2001)029<0991:OBAEAT>2.0.CO;2

Weil, A. B., & Yonkee, A. (2009). Anisotropy of magnetic susceptibility in weakly deformed red beds from the Wyoming salient, Sevier thrust belt: Relations to layer-parallel shortening and orogenic curvature. *Lithosphere*, *1*(4), 235–256. https://doi.org/10.1130/L42.1

Weil, A. B., Yonkee, A., & Sussman, A. (2010). Reconstructing the kinematic evolution of curved mountain belts: A paleomagnetic study of Triassic red beds from the Wyoming salient, Sevier thrust belt, U.S.A. *GSA Bulletin*, *122*(1–2), 3–23. https://doi.org/10.1130/B26483.1

Wengler, M., Barboza-Gudiño, J., Thomsen, T., & Meinhold, G. (2019). Sediment provenance of Triassic and Jurassic sandstones in central Mexico during activity of the Nazas volcanic arc. *Journal of South American Earth Sciences*, *92*, 329–349. https://doi.org/10.1016/j.jsames.2019.03.009

Williams, S. A., Singleton, J. S., Prior, M. G., Mavor, S. P., Cross, G. E., & Stockli, D. F. (2021). The early Palaeogene transition from thin-skinned to thick-skinned shortening in the Potosí uplift, Sierra Madre Oriental, northeastern Mexico. *International Geology Review*, *63*(2), 233–263. https://doi.org/10.1080/00206814.2020.1805802

Wilson, P., McCaffrey, K., Wilson, R., Jarvis, I., & Holdsworth, R. (2016). Deformation structures associated with the Trachyte Mesa intrusion, Henry Mountains, Utah: Implications for sill and laccolith emplacement mechanisms. *Journal of Structural Geology*, *87*, 30–46. https://doi.org/10.1016/j.jsg.2016.04.001

Yonkee, A., & Weil, A. B. (2010). Reconstructing the kinematic evolution of curved mountain belts: Internal strain patterns in the Wyoming salient, Sevier thrust belt, U.S.A. *GSA Bulletin*, *122*(1–2), 24–49. https://doi.org/10.1130/B26484.1

Zachary, D. W. (2012). *Stratigraphic controls on the structural evolution of the Sierra Madre oriental fold-thrust belt, eastern Mexico [Msc Thesis]*. University of Houston.

Zavala-Monsiváis, A., Barboza-Gudiño, J. R., Velasco-Tapia, F., & García-Arreola, M. E. (2012). Sucesión volcánica Jurásica en el área de Charcas, San Luis Potosí: Contribución al entendimiento del Arco Nazas en el noreste de Mexico. *Boletín de La Sociedad Geológica Mexicana*, *64*(3), 277–293. https://doi.org/10.18268/bsgm2012v64n3a2

Zhou, Y., Murphy, M. A., & Hamade, A. (2006). Structural development of the Peregrina–Huizachal anticlinorium, Mexico. *Journal of Structural Geology*, *28*(3), 494–507. https://doi.org/10.1016/j.jsg.2005.11.005

Zijderveld, J. D. A. (1967). *AC demagnetization of rocks: Analysis of results, methods in paleomagnetism DW collinson, KM Creer, SK Runcorn* (pp. 254–286). Elsevier.